

# SoRoTop: a hitchhiker’s guide to topology optimization MATLAB code for design-dependent pneumatic-driven soft robots

Prabhat Kumar<sup>1</sup>

*Department of Mechanical and Aerospace Engineering, Indian Institute of Technology Hyderabad, 502285, India*

Published<sup>2</sup> in *Optimization and Engineering*, DOI:10.1007/s11081-023-09865-1

Submitted on 14 June 2023, Revised on 14 October 2023, Accepted on 14 October 2023

---

**Abstract:** Demands for pneumatic-driven soft robots are constantly rising for various applications. However, they are often designed manually due to the lack of systematic methods. Moreover, design-dependent characteristics of pneumatic actuation pose distinctive challenges. This paper provides a compact MATLAB code, named SoRoTop, and its various extensions for designing pneumatic-driven soft robots using topology optimization. The code uses the method of moving asymptotes as the optimizer and builds upon the approach initially presented in Kumar et al. (*Struct Multidiscip Optim* 61 (4): 1637–1655, 2020). The pneumatic load is modeled using Darcy’s law with a conceptualized drainage term. Consistent nodal loads are determined from the resultant pressure field using the conventional finite element approach. The robust formulation is employed, i.e., the eroded and blueprint design descriptions are used. A min-max optimization problem is formulated using the output displacements of the eroded and blueprint designs. A volume constraint is imposed on the blueprint design, while the eroded design is used to apply a conceptualized strain energy constraint. The latter constraint aids in attaining optimized designs that can endure the applied load without compromising their performance. Sensitivities required for optimization are computed using the adjoint-variable method. The code is explained in detail, and various extensions are also presented. It is structured into pre-optimization, MMA optimization, and post-optimization operations, each of which is comprehensively detailed. The paper also illustrates the impact of load sensitivities on the optimized designs. SoRoTop is provided in Appendix A and is available with extensions in the supplementary material and publicly at <https://github.com/PrabhatIn/SoRoTop>.

**Keywords:** Pneumatically driven soft robots; design-dependent loads; Topology optimization; Robust formulation; MATLAB code

---

## 1 Introduction

Robotics has gained unprecedented attention and development across various applications, including industry, academia, household chores, official tasks, and defense applications, to name a few. Additionally, there is a growing interest in “soft robotics” due to its unique advantages over traditional rigid robots that rely on solid linkage mechanisms. Soft robots are designed using materials with Young’s modulus ranging from kilopascals to megapascals. These robots perform tasks by utilizing the deformation of their flexible bodies, making them well-suited for various purposes, such as human interaction in unstructured and dynamic environments, fragile objects handling, fruit and vegetable picking and placing, and achieving high power-to-weight ratios (Kumar, 2022; Xavier et al., 2022). Thus, nowadays, they find various applications in, e.g., gripping (Xie et al., 2020; Pinskiier et al., 2023), sensing (Zhao et al.,

---

<sup>1</sup>pkumar@mae.iith.ac.in

<sup>2</sup>This pdf is the personal version of an article whose final publication is available at [Optimization and Engineering](#)

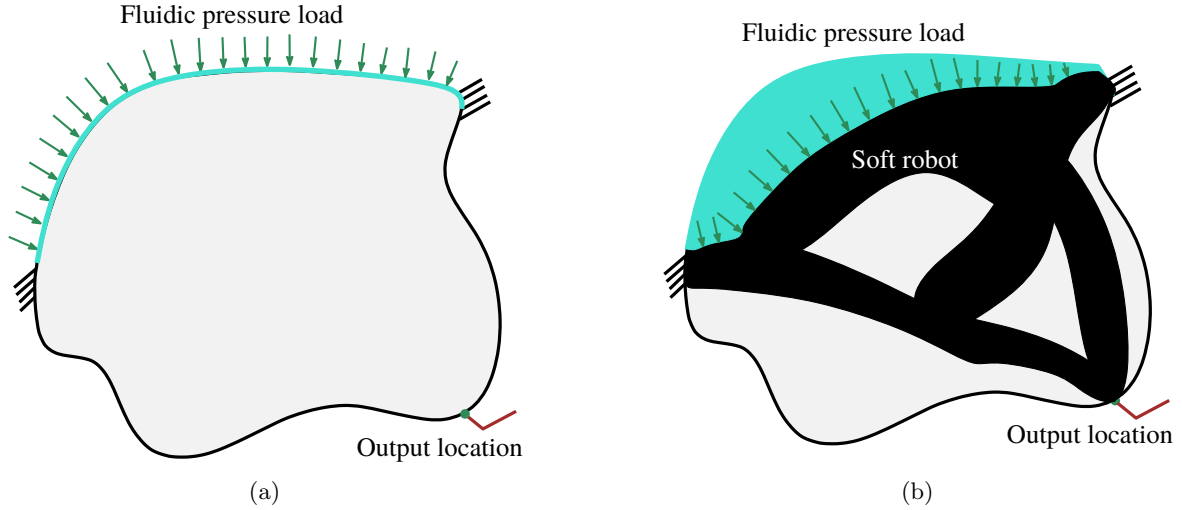


Figure 1: A schematic diagram for a pressure-driven soft robot. (a) Design domain. A set of arrows indicates the fluidic pressure load. Fixed boundary conditions are also depicted. (b) A representative solution. One notices that pressure

2016), invasive surgery (Hu et al., 2018), rehabilitation (Polygerinos et al., 2013), handling soft and fragile objects (Shintake et al., 2018; Deimel and Brock, 2013), and human-robot interaction (Deimel and Brock, 2013), etc. These robots can be classified based on the ways they require actuation. For example, fluidic pressure-driven actuation (Kumar et al., 2020; Kumar, 2022; Gorissen et al., 2017; Kumar and Langelaar, 2022; de Souza and Silva, 2020; Lu and Tong, 2021; Vasista and Tong, 2012), cable-driven actuation (Chen et al., 2018), electroactive polymer-based actuation (Pourazadi et al., 2019) and shape-memory material-based actuation (Jin et al., 2016), etc. Among these, fluidic pressure (pneumatic)-driven robots are more sought after because of their lightweight, quick response, and low-cost components (Kumar, 2022; Xavier et al., 2022). However, due to a lack of systematic approaches, they are designed manually using heuristic methods that heavily depend on designers’ knowledge, experience, and expertise. Such heuristic methods often require numerous resources/iterations to achieve the desired designs; thus, they introduce limitations and may not be efficient.

Characteristic features of soft robots resemble those of compliant mechanisms that perform their tasks utilizing the motion obtained from their flexible members (Kumar, 2022). Thus, topology optimization methods for designing pneumatically actuated compliant mechanisms (CMs) can be one of the promising ways to design soft robots (Kumar and Langelaar, 2022; Kumar, 2022). Topology optimization (TO), a computational technique, determines where to place material and where to make holes (void) within a given design domain to achieve optimum performance. The design domain is typically parameterized using finite elements (FEs), and each element is assigned a design variable  $\rho \in [0, 1]$ .  $\rho_i = 1$  indicates material or solid phase while  $\rho_i = 0$  denotes void state of element  $i$ . The optimized designs are expected to contain FEs with  $\rho = 1$ . However, the TO problem is often relaxed in practical applications, leading to optimized designs that may include elements with  $0 < \rho < 1$  (Sigmund and Maute, 2013). To mitigate this and guide solutions toward 0-1, the Heaviside projection-based filter can be employed (Wang et al., 2011).

A design-dependent load changes its magnitude, direction, and/or location as topology advances (Kumar et al., 2020). Therefore, such loads pose several unique challenges within a TO setting (Kumar et al., 2020; Hammer and Olhoff, 2000; Kumar, 2023). These challenges encompass: (a) locating the boundary to apply the pneumatic load, which involves relating the pressure field to the employed design variables, (b) converting the fluidic pressure field into consistent nodal loads, and (c) effectively evaluating the load sensitivities. These challenges can become more prominent when designing pneumatic-activated soft robots/compliant mechanisms (Kumar et al., 2020; Kumar and Langelaar, 2021). Fig. 1a displays a schematic diagram, and Fig. 1b depicts its representative optimized soft robots design. One notes that the pressure boundary changes, and the load’s direction, magnitude,

and location get updated. Typically, soft robots experience large deformation while performing their tasks. Elements/regions with low stiffness deform significantly; thus, they pose an additional set of challenges (Wang et al., 2014; Kumar et al., 2021). In addition, for capturing the design-dependent nature of the pneumatic loads with large deformation, one needs to include the follower force concepts within the formulation (Kumar and Langelaar, 2022). Moreover, when designing mechanisms, there may be instances where members come into contact with each other, further complicating the formulation (Kumar et al., 2019). Given the various nonlinearities and complexities associated with these challenges, it is worth noting that the discussion in this paper is confined to a linear and standard finite element setting, and detailed discussions of each nonlinearity are beyond the scope of the provided MATLAB code.

Hammer and Olhoff (2000) were the first to present fluid pressure load within the TO setting for designing loadbearing structures. Since then, many approaches have been developed to explicitly design loadbearing structures by minimizing their compliance; see Refs. (Kumar et al., 2020; Picelli et al., 2019; Kumar and Langelaar, 2021) and related reference therein for a detailed overview. Hiller and Lipson (2011) employed the evolutionary TO method to design soft robots, while Chen et al. (2018) utilized level-set TO to create a soft cable-driven gripper. Zhang et al. (2018) designed a soft pneumatic gripper. However, none of the methods in these studies (Hiller and Lipson, 2011; Chen et al., 2018; Zhang et al., 2018) considered for the design-dependent characteristics of the pneumatic loads in their approaches. Recently, Pinskiier et al. (2023) presented TO methods for 3D multi-material soft grippers building upon the first introduced in (Kumar et al., 2020; Kumar and Langelaar, 2021). In addition, to date, only a limited number of TO methods exist to design fluidic pressure-actuated compliant mechanisms considering the design-dependent nature of the loads in 2D (Kumar et al., 2020; Kumar and Langelaar, 2022; Panganiban et al., 2010; Vasista and Tong, 2012; de Souza and Silva, 2020; Lu and Tong, 2021) and 3D (Panganiban et al., 2010; Kumar and Langelaar, 2021) settings. Given the various challenges and complexities involved in these approaches, newcomers, students and even experienced researchers in this field may face difficulties in developing new approaches or using existing ones. Therefore, to facilitate their learning and research, we need a freely available systematic MATLAB code for designing pneumatically actuated soft robots.

Providing open codes and sub-routines within research communities is highly appreciated, as they greatly facilitate the hands-on experience and efficient learning of the (new) concepts. The codes also facilitate reproducibility and provide confidence in the outcomes. In the current state-of-the-art of TO, readers can find numerous MATLAB codes for different applications such as (Kumar, 2023; Sigmund, 2001; Suresh, 2010; Andreassen et al., 2011; Ferrari et al., 2021; Picelli et al., 2021; Homayouni-Amlashi et al., 2021; Gao et al., 2019; Ali and Shimoda, 2022; Alexandersen, 2023; Kumar, 2023). For an in-depth review of such educational codes, refer to Wang et al. (2021). Despite the increasing interest in automated methods for designing pneumatic-driven soft robots, no open-source codes are currently available. Therefore, there is a significant need for open-source MATLAB codes in this field to support the growing research interest and educational needs.

This paper aims to provide a MATLAB code for systematically designing pneumatic-driven soft robots to ease the learning in this field. The code is also expected to furnish a suitable platform for researchers to develop, explore, and extend for designing various soft robots for different applications.

The presented code, named **SoRoTop**, is developed using the approach initially introduced in Kumar et al. (2020) and **TOPress** MATLAB code (Kumar, 2023). The density-based TO setting is considered. We use the robust formulation (Wang et al., 2011) with blueprint (intermediate) and eroded designs, i.e., the optimized mechanisms are robust regarding over-etching (see Fig. 2). Over-etching involves exposing the substrate to an etching process longer than necessary to remove excess material. The method of moving asymptotes (MMA, written in 1999 and updated in the 2002 version) (Svanberg, 1987) is used as the optimizer, allowing users to extend the code with additional physics and multiple constraints readily. A noteworthy aspect of the code is its consideration of load sensitivities. Load sensitivities exist due to the design-dependent nature of the load as discussed in (Kumar et al., 2020;

Kumar, 2023). The code also demonstrates the importance and effects of load sensitivities on the optimized mechanisms.

The remainder of the paper is structured as follows. Sec. 2 models pressure load as a design-dependent force and evaluates the consistent nodal forces. Sec. 3 describes topology optimization formulation, wherein the robust optimization scheme is described and sensitivity analysis is performed. MATLAB implementation for SoRoTop code is described in detail in Sec. 4. Numerical results using SoRoTop are presented in Sec. 5. Various extensions of SoRoTop are provided for different pneumatically actuated soft mechanisms. The section also provides discussions on these results. Lastly, concluding remarks are presented in Sec. 6.

## 2 Pressure load modeling and nodal forces evaluation

We confine ourselves to density-based TO (Sigmund and Maute, 2013) herein. Thus, each element is assigned a design (density) variable considered constant within the element. Typically, optimization starts by initializing the element's density equal to the allowed element volume fraction,  $\frac{V^*}{nel}$ .  $V^*$  represents the total volume fraction, and  $nel$  indicates the total number of square bi-linear finite elements to parameterize the design domain. Next, we briefly describe the modeling of pressure load and evaluation of consistent nodal force evaluation for the sake of completeness. One may refer to Kumar et al. (2020) for a detailed description.

### 2.1 Design-dependent pressure load modeling

As optimization progresses, material phases of elements change, and elements can be considered a porous medium. In addition, for the given design problem, the fluidic pressure boundary conditions are known *a priori*. Therefore, per Kumar et al. (2020); Kumar and Langelaar (2021), Darcy law is a natural and appropriate choice to model pressure load or to establish the relationship between pressure load and the design variables. The Darcy flux  $\mathbf{q}$  is determined as

$$\mathbf{q} = -\frac{\kappa}{\mu}\nabla p = -K(\bar{\rho})\nabla p, \quad (1)$$

where  $\nabla p$ ,  $\kappa$ , and  $\mu$  represent the pressure gradient, permeability of the medium, and fluid viscosity, respectively.  $\bar{\rho}$  is the physical variable, and  $K(\bar{\rho})$  is termed flow coefficient. The latter is related to the former for element  $e$  as

$$K(\bar{\rho}_e) = K_v(1 - (1 - \epsilon)\mathcal{H}(\bar{\rho}_e, \beta_\kappa, \eta_\kappa)), \quad (2)$$

where  $\epsilon = \frac{K_s}{K_v}$  is the flow contrast.  $K_v$  and  $K_s$  are the flow coefficients of the void and solid phases of an element.

$$\mathcal{H}(\bar{\rho}_e, \beta_\kappa, \eta_\kappa) = \frac{\tanh(\beta_\kappa\eta_\kappa) + \tanh(\beta_\kappa(\bar{\rho}_e - \eta_\kappa))}{\tanh(\beta_\kappa\eta_\kappa) + \tanh(\beta_\kappa(1 - \eta_\kappa))} \quad (3)$$

is a smooth Heaviside function.  $\eta_\kappa$  defines transition point, whereas  $\beta_\kappa$  indicates steepness for the flow coefficient. We set  $K_v = 1$ , and  $\epsilon = 1 \times 10^{-7}$  (Kumar and Langelaar, 2021; Kumar, 2023). Solving Eq. 1 may not give the realistic pressure variation as demonstrated in Kumar and Langelaar (2021); Kumar and Saxena (2022); Kumar (2023). Thus, the additional volumetric drainage term  $Q_{\text{drain}}$  is conceptualized and included in the Darcy law. Now, the balance equation can be written as

$$\nabla \cdot \mathbf{q} - Q_{\text{drain}} = \nabla \cdot (K(\bar{\rho})\nabla p) + Q_{\text{drain}} = 0, \quad (4)$$

where  $Q_{\text{drain}} = -D(\bar{\rho}_e)(p - p_{\text{ext}})$  with

$$D(\bar{\rho}_e) = D_s\mathcal{H}(\bar{\rho}_e, \beta_d, \eta_d), \quad (5)$$

where  $\{\eta_d, \beta_d\}$  are the drainage parameters.  $\eta_d$  and  $\beta_d$  define the transition and steepness for the drainage term, respectively.  $p_{\text{ext}}$  is the external pressure field. Per Kumar et al. (2020),  $D_s = \left(\frac{\ln r}{\Delta s}\right)^2 K_s$ , where  $r = \frac{p|\Delta s}{p_{\text{in}}}$ .  $p|\Delta s$  is the pressure at  $\Delta s$ , a penetration parameter set to the width/height of a few FEs (Kumar et al., 2020). In general,  $r \in [0.001 \ 0.1]$  is set. Per Kumar (2023), user-defined parameters are reduced by considering  $\eta_d = \eta_k = \eta_f$  and  $\beta_d = \beta_k = \beta_f$  for the provided code, SoRotop. We indicate  $\eta_f$  and  $\beta_f$  in SoRotop by `etaf` and `betaf`, respectively.

Equation 4 is solved using the standard finite element method, that transpires to (Kumar et al., 2020; Kumar, 2023)

$$\mathbf{K}_p^e \mathbf{p}_e + \mathbf{K}_{Dp}^e \mathbf{p}_e = \mathbf{A}_e \mathbf{p}_e = \mathbf{0}, \quad (6)$$

where  $\mathbf{K}_p^e$  is the element flow matrix due to Darcy law, whereas  $\mathbf{K}_{Dp}^e$  appears due to the drainage term.  $\mathbf{A}_e$  indicates the overall element flow matrix. With the global flow matrix  $\mathbf{A}$  and global pressure field  $\mathbf{p}$ , Eq. 6 is written as

$$\mathbf{A} \mathbf{p} = \mathbf{0}. \quad (7)$$

One solves Eq. 7 using the given pressure boundary conditions to obtain the overall pressure field  $\mathbf{p}$ .  $\mathbf{A}$  and  $\mathbf{p}$  are sub-blocked into *free* and *prescribed*, denoted using subscripts  $f$  and  $p$ , respectively; thus, Eq. 7 can be written as

$$\begin{bmatrix} \mathbf{A}_{ff} & \mathbf{A}_{fp} \\ \mathbf{A}_{fp}^\top & \mathbf{A}_{pp} \end{bmatrix} \begin{bmatrix} \mathbf{p}_f \\ \mathbf{p}_p \end{bmatrix} = \begin{bmatrix} \mathbf{0} \\ \mathbf{0} \end{bmatrix}. \quad (8)$$

The first row of Eq. 8 yields  $\mathbf{p}_f = \mathbf{A}_{ff}^{-1} \mathbf{A}_{fp} \mathbf{p}_p$ ; thus, the pressure field  $\mathbf{p}$  is determined.

## 2.2 Nodal forces evaluation

The nodal forces are obtained from the pressure field as (Kumar et al., 2020)

$$\mathbf{b} dV = -\nabla p dV, \quad (9)$$

where  $dV$  is the infinitesimal volume and  $\mathbf{b}$  is the body force (Kumar et al., 2020). Now, using the standard FE method, one writes at the elemental level

$$\mathbf{F}_e = - \left[ \int_{\Omega_e} \mathbf{N}_u^\top \mathbf{B}_p dV \right] \mathbf{p}_e = -\mathbf{T}_e \mathbf{p}_e, \quad (10)$$

where  $\mathbf{N}_u = [N_1 \mathbf{I}, N_2 \mathbf{I}, N_3 \mathbf{I}, N_4 \mathbf{I}]$ , with  $N_1, N_2, N_3, N_4$  are the bi-linear shape functions,  $\mathbf{B}_p^\top = \nabla \mathbf{N}_p$  with  $\mathbf{N}_p = [N_1, N_2, N_3, N_4]^\top$  and  $\mathbf{I}$  is the identity matrix in  $\mathcal{R}^2$ .  $\mathbf{T}_e$  is called the transformation matrix.  $\mathbf{p}_e$  is the elemental pressure vector, i.e.,  $\mathbf{p}_e = [p_1, p_2, p_3, p_4]^\top$ . In the global sense, Eq. 10 transpire to

$$\mathbf{F} = -\mathbf{T} \mathbf{p}, \quad (11)$$

where  $\mathbf{F}$  and  $\mathbf{T}$  are the global force vector and transformation matrix, respectively. For the given problem, one uses Eq. 7 to determine the overall pressure field in view of the given pressure boundary conditions, whereas Eq. 11 is used to determine the global nodal forces from the obtained pressure field  $\mathbf{p}$ .

## 3 Topology optimization formulation

We use the modified SIMP formulation (Sigmund and Maute, 2013) to interpolate the Young's modulus defined for element  $i$  as,

$$E_i = E_{\min} + \bar{\rho}_i^p (E_1 - E_{\min}), \quad (12)$$

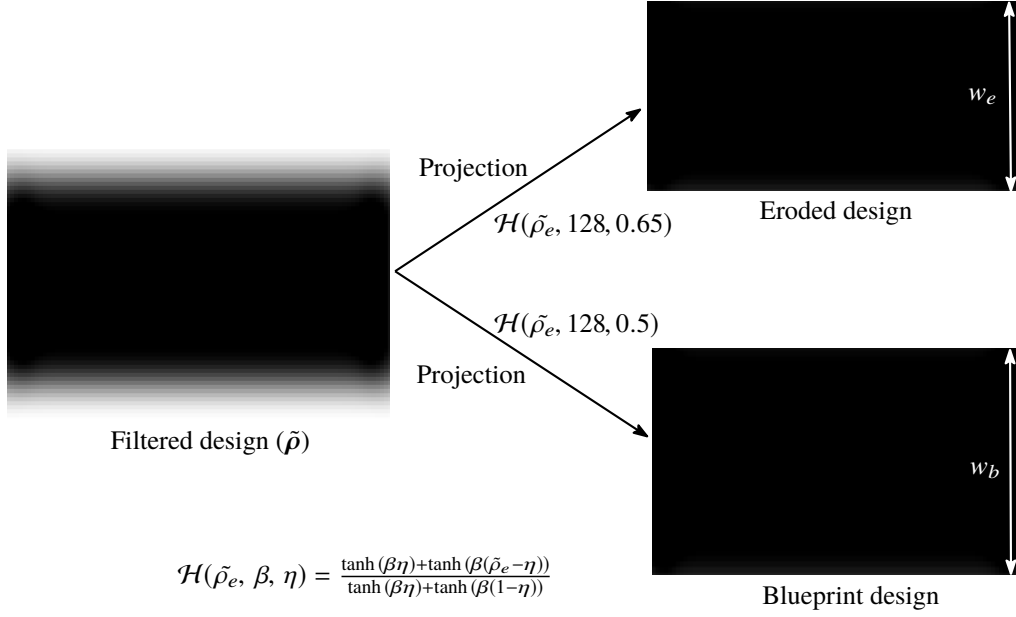


Figure 2: A schematic for filtered, eroded and blueprint designs.  $w_e < w_b$ , where  $w_e$  and  $w_b$  represent the widths of the eroded ( $\eta = 0.65$ ) and blueprint designs ( $\eta = 0.5$ ), respectively.

where  $E_1$  and  $E_{\min}$  are Young's moduli of the solid and void phases of an element, respectively, and  $E_i$  is interpolated Young's modulus of element  $i$ .  $E_{\min}$  is assigned to the void elements to avoid the singularity of the structural stiffness matrix during finite element solve.  $p$  is the SIMP parameter.  $\bar{\rho}$ , the physical design variable of element  $i$ , is determined as

$$\bar{\rho}_i = \frac{\tanh(\beta\eta) + \tanh(\beta(\tilde{\rho}_i - \eta))}{\tanh(\beta\eta) + \tanh(\beta(1 - \eta))} = \mathcal{H}(\tilde{\rho}_i, \beta, \eta), \quad (13)$$

where  $\eta$  indicates the transition point and  $\beta \in (0, \infty)$  represents the steepness parameter, for values greater than 0, it reduces the number of gray elements. To achieve binary optimized solutions,  $\beta$  is increased towards infinity. However, for  $\beta \rightarrow \infty$ ,  $\frac{\partial \bar{\rho}_i}{\partial \tilde{\rho}_i} \rightarrow 0$ , i.e., derivatives of the objective become very small; thus jeopardize the optimization progress. The choice of starting  $\beta$  can vary; initializing with a higher number hinders the optimization search behavior due to the abovementioned reasons. Thus, we start with  $\beta = 1$  and increase it in a continuation fashion till  $\beta_{\max} = 128$ . The derivative of  $\bar{\rho}$  with respect to the  $\tilde{\rho}$  can be determined as

$$\frac{\partial \bar{\rho}_i}{\partial \tilde{\rho}_i} = \beta \frac{1 - \tanh(\beta(\tilde{\rho} - \eta))^2}{(\tanh(\beta\eta) + \tanh(\beta(1 - \eta)))^2}, \quad (14)$$

$\tilde{\rho}$  denotes the filtered design variable for element  $i$ . Mathematically, we evaluate  $\tilde{\rho}$  as

$$\tilde{\rho}_i = \frac{\sum_{j=1}^{nel} \rho_j v_j w(\mathbf{x}_i, \mathbf{x}_j)}{\sum_{j=1}^{nel} v_j w(\mathbf{x}_i, \mathbf{x}_j)}, \quad (15)$$

where  $w(\mathbf{x}_i, \mathbf{x}_j) = \max\left(0, 1 - \frac{\|\mathbf{x}_i - \mathbf{x}_j\|}{r_{\text{fill}}}\right)$  (Bruns and Tortorelli, 2001). The filter radius is indicated by  $r_{\text{fill}}$ .  $v_j$  represents volume of element  $j$ .  $w(\mathbf{x}_i, \mathbf{x}_j)$  is determined at the beginning of the optimization, as it does not alter with TO iterations. It is stored in a matrix  $\mathbf{Hs}$  in the following manner:

$$\mathbf{Hs}_{i,j} = \frac{v_j w(\mathbf{x}_i, \mathbf{x}_j)}{\sum_{j=1}^{nel} v_j w(\mathbf{x}_k, \mathbf{x}_j)}. \quad (16)$$

Finally, the filtering process is performed as  $\tilde{\rho} = \mathbf{H}\mathbf{s}\rho$ , and one determines its derivative with respect to  $\rho$  as

$$\frac{\partial \tilde{\rho}}{\partial \rho} = \mathbf{H}\mathbf{s}^\top. \quad (17)$$

One may also use `infilter` MATLAB function for performing the filtering operations (Ferrari et al., 2021; Kumar, 2023).

### 3.1 Optimization problem formulation

The optimized CMs obtained using topology optimization typically contain single-node connections (Sigmund, 1997; Yin and Ananthasuresh, 2003). These connections show artificial stiffness, permit load transfer with zero stiffness, and appear due to deficiencies in FE-analysis with quadrilateral elements. CMs with such hinges are difficult to realize as, in reality, compliant hinges will always have finite rotational stiffness. Numerous methods have been proposed to circumvent the introduction of point connections in the optimized CMs (Yin and Ananthasuresh, 2003; Poulsen, 2003; Saxena and Saxena, 2007; Wang et al., 2011; Singh et al., 2020). Herein, we use the robust formulation (Wang et al., 2011) with respect to the blueprint and eroded designs (Kumar and Langelaar, 2022). We replace  $\eta$  by  $0.5 + \Delta\eta$  and  $0.5$  in Eq. 13 for determining the eroded and blueprint variables, respectively (Fig. 2 cf. Wang et al. (2011)).  $\Delta\eta \in [0, 0.5]$  is a user-defined parameter.

As mentioned before, the characteristics of soft robots (monolithic designs with no rigid joints) are similar to CMs (Kumar, 2022). TO of CMs for achieving maximum output displacements with the design-dependent behavior of the pneumatic loads can be one of the promising directions to design soft robots (Kumar, 2022; de Souza and Silva, 2020; Pinskiier et al., 2023). A min-max, non-smooth optimization problem is formulated using the output deformation of the blueprint and eroded designs. The given volume constraint is applied to the blueprint design. This indicates that the optimized result is robust with respect to the over-etching (Wang et al., 2011; Fernández et al., 2020). The optimized mechanisms are expected to sustain under the applied loads (Saxena and Ananthasuresh, 2000); therefore, a strain energy constraint is conceptualized and applied to the eroded design. The constraint aids in attaining optimized designs that can endure the applied load without compromising their performance. The optimization problem is solved using the method of moving asymptotes (MMA, cf. Svanberg (1987)). Mathematically, the optimization problem is written as

$$\left. \begin{aligned} \min_{\tilde{\rho}(\tilde{\rho}(\rho))} : f_0 = \max_r u_r^{\text{out}} = \max_r \left\{ \mathbf{l}^\top \mathbf{u}_r \right\} |_{r=e,b} \\ \text{such that:} \\ {}^1 \boldsymbol{\lambda}_r : \mathbf{A}_r \mathbf{p}_r = \mathbf{0} \\ {}^2 \boldsymbol{\lambda}_r : \mathbf{K}_r \mathbf{u}_r = \mathbf{F}_r = -\mathbf{T} \mathbf{p}_r \\ \Lambda_b : g_1 = \frac{V_b}{V^*} - 1 \leq 0 \\ \Lambda_e : g_2 = \frac{SE_e}{SE^*} - 1 \leq 0 \\ 0 \leq \rho_i, \tilde{\rho}_i, \bar{\rho}_i \leq 1 \quad \forall i \end{aligned} \right\}, \quad (18)$$

where quantities with subscript  $e$  and  $b$  are related to the eroded and intermediate/blueprint designs, respectively (Wang et al., 2011; Kumar and Langelaar, 2022).  $\mathbf{u}_r$  is the global displacement vector, whereas  $\mathbf{K}_r$  indicates the global stiffness matrix.  $u_r^{\text{out}}$  denotes the output displacement of the mechanisms in the desired directions.  $\mathbf{l}$  is a vector with all zeros except the entry corresponding to the output degree of freedom set to one.  $V^*$  and  $V_b$  are the blueprint design's permitted and current volume fractions, respectively.  $SE_e$  and  $SE^*$  are the eroded design's current and defined strain energy,



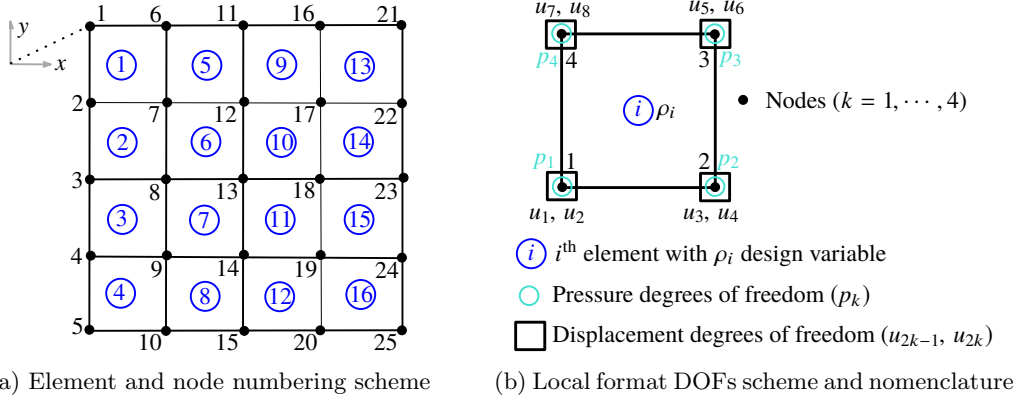


Figure 3: Figure displays the mesh grid format (element and node numbering scheme) and nomenclature of element  $i$ . (a)  $\text{nlex} = 4$ ,  $\text{nley} = 4$ ,  $\text{Lnode} = 1, 2, 3, 4, 5$ ,  $\text{Tnode} = 1, 6, 11, 16, 21$ ,  $\text{Rnode} = 21, 22, 23, 24, 25$ ,  $\text{Bnode} = 5, 10, 15, 20, 25$ ;  $\text{nlex}$  and  $\text{nley}$  represent the number of elements in  $x$ - and  $y$ -directions, respectively.  $\text{Lnode}$ ,  $\text{Rnode}$ ,  $\text{Tnode}$ , and  $\text{Bnode}$  denote nodes constituting left, right, top, and bottom edges, respectively. (b) Local format DOFs scheme and nomenclature of element  $i$ . Each node is characterized by two displacements and one pressure degree of freedom.

respectively. We choose  $SE^*$  at the initial optimization stage so that the optimized mechanism can sustain the applied load and deliver high performance. The  $SE^*$  and  $g_2$  are determined as

---

**Algorithm 1** Calculation of  $SE^*$  and  $g_2$  formulation

---

**Require:**  $loop$ ,  $\mathbf{u}_e$ ,  $\mathbf{K}_e$ ,  $SE_e = \frac{1}{2} \mathbf{u}_e^\top \mathbf{K}_e \mathbf{u}_e$

**if**  $loop == 1$  **then**

$SE^* = S_f \times SE_e$

**end if**

$g_2 = \frac{SE_e}{SE^*} - 1 \leq 0$

---

where  $S_f$ , a user-defined strain energy fraction, is selected to obtain a sustainable/realizable mechanism. Our numerical experiments and experience show that  $S_f \in [0.85, 0.95]$  works fine; however, a user can use different  $S_f$  as per the applications. The formulation requires solving four forward (two for flow and two for structure) problems and three adjoints (one for each objective and one for  $g_2$ ).

### 3.2 Sensitivity analysis

This section provides the sensitivity analyses for the objective and constraint functions. The derivatives of these functions are determined using the adjoint-variable method. One can write the augmented performance function  $\mathcal{L}_0$  for the objective as

$$\mathcal{L}_0 = f_0 + {}^1\lambda_r^\top (\mathbf{A}_r \mathbf{p}_r) + {}^2\lambda_r^\top (\mathbf{K}_r \mathbf{u}_r + \mathbf{T} \mathbf{p}_r), \quad (19)$$



Differentiating Eq. 19 with respect to the physical design variable  $\bar{\rho}_r$ , one gets

$$\begin{aligned}
\frac{\partial \mathcal{L}_0}{\partial \bar{\rho}_r} &= \frac{\partial f_0}{\partial \bar{\rho}_r} + \frac{\partial f_0}{\partial \mathbf{u}_r} \frac{\partial \mathbf{u}_r}{\partial \bar{\rho}_r} + {}^1\boldsymbol{\lambda}_r^\top \left( \frac{\partial \mathbf{A}_r}{\partial \bar{\rho}_r} \mathbf{p}_r \right) \\
&\quad + {}^1\boldsymbol{\lambda}_r^\top \left( \mathbf{A}_r \frac{\partial \mathbf{p}_r}{\partial \bar{\rho}_r} \right) + {}^2\boldsymbol{\lambda}_r^\top \left( \frac{\partial \mathbf{K}_r}{\partial \bar{\rho}_r} \mathbf{u}_r + \mathbf{K}_r \frac{\partial \mathbf{u}_r}{\partial \bar{\rho}_r} \right) \\
&\quad + {}^2\boldsymbol{\lambda}_r^\top \left( \frac{\partial \mathbf{T}}{\partial \bar{\rho}_r} \mathbf{p}_r + \mathbf{T} \frac{\partial \mathbf{p}_r}{\partial \bar{\rho}_r} \right) \\
&= \frac{\partial f_0}{\partial \bar{\rho}_r} + {}^2\boldsymbol{\lambda}_r^\top \left( \frac{\partial \mathbf{K}_r}{\partial \bar{\rho}_r} \mathbf{u}_r \right) + {}^1\boldsymbol{\lambda}_r^\top \left( \frac{\partial \mathbf{A}_r}{\partial \bar{\rho}_r} \mathbf{p}_r \right) \\
&\quad + \underbrace{\left( \mathbf{l}^\top + {}^2\boldsymbol{\lambda}_r^\top \mathbf{K}_r \right)}_{\mathcal{T}_1} \frac{\partial \mathbf{u}_r}{\partial \bar{\rho}_r} + \underbrace{\left( {}^1\boldsymbol{\lambda}_r^\top \mathbf{A}_r + {}^2\boldsymbol{\lambda}_r^\top \mathbf{T} \right)}_{\mathcal{T}_2} \frac{\partial \mathbf{p}_r}{\partial \bar{\rho}_r}.
\end{aligned} \tag{20}$$

With respect to the fundamentals of the adjoint-variable method, one chooses  ${}^1\boldsymbol{\lambda}_r$  and  ${}^2\boldsymbol{\lambda}_r$  such that  $\mathcal{T}_1 = 0$  and  $\mathcal{T}_2 = 0$ , which give

$${}^2\boldsymbol{\lambda}_r^\top = -\mathbf{l}^\top \mathbf{K}_r^{-1}, \quad {}^1\boldsymbol{\lambda}_r^\top = -{}^2\boldsymbol{\lambda}_r^\top \mathbf{T} \mathbf{A}_r^{-1} = \mathbf{l}^\top \mathbf{K}_r^{-1} \mathbf{T} \mathbf{A}_r^{-1}. \tag{21}$$

Note that  $\frac{\partial f_0}{\partial \bar{\rho}_r} = 0$ , thus, we get

$$\begin{aligned}
\frac{\partial f_0}{\partial \bar{\rho}_r} &= -\mathbf{l}^\top \mathbf{K}_r^{-1} \frac{\partial \mathbf{K}_r}{\partial \bar{\rho}_r} \mathbf{u}_r + \underbrace{\mathbf{l}^\top \mathbf{K}_r^{-1} \mathbf{T} \mathbf{A}_r^{-1} \frac{\partial \mathbf{A}_r}{\partial \bar{\rho}_r} \mathbf{p}_r}_{\text{Load sensitivities}}.
\end{aligned} \tag{22}$$

One notes that load sensitivities alter the total objective sensitivity (Eq. 22). In the case of constant actuating scenarios, only the first term in Eq. 22 appears. Likewise, one finds the derivative of constraint  $g_2$  with respect to the physical design vector as

$$\frac{\partial g_2}{\partial \bar{\rho}_r} = \frac{-\frac{1}{2} \mathbf{u}_r^\top \frac{\partial \mathbf{K}_r}{\partial \bar{\rho}_r} \mathbf{u}_r + \mathbf{u}_r^\top \mathbf{T} \mathbf{A}_r^{-1} \frac{\partial \mathbf{A}_r}{\partial \bar{\rho}_r} \mathbf{p}_r}{SE^*}, \tag{23}$$

where  $SE^*$  is the permitted strain energy (see Alg. 1). Determining the derivative of  $g_1$  is straightforward (Kumar, 2023). Finally, we use the chain rule to determine the objective and constraints derivatives with respect to the design variable as

$$\frac{\partial f}{\partial \boldsymbol{\rho}_r} = \frac{\partial f}{\partial \bar{\rho}_r} \frac{\partial \bar{\rho}_r}{\partial \boldsymbol{\rho}_r}, \tag{24}$$

where  $f$  represents objective/constraint functions. One uses Eq. 22 and Eq. 23 to determine  $\frac{\partial f}{\partial \bar{\rho}_r}$ .  $\frac{\partial \bar{\rho}_r}{\partial \boldsymbol{\rho}_r}$  and  $\frac{\partial \bar{\rho}_r}{\partial \boldsymbol{\rho}_r}$  are determined using Eq. 14 and Eq. 17, respectively. Next, we discuss the implementation of the MATLAB code, SoRoTop.

## 4 MATLAB implementation

This section provides a detailed description of the presented code, SoRoTop. The code (Appendix A) and its extensions for different soft mechanisms are provided as supplementary material to the paper. One can call the code from the MATLAB command window as

---

```
SoRoTop(nelx, nely, volfrac, sefrac, penal, rmin, kss, etaf, betaf, lst, betamax, delrbst, maxit)
```

---

where `nelx` and `nely` are the number of elements in the  $x$ - and  $y$ -directions, respectively, `volfrac` (Eq. 18) indicates the permitted volume fraction, `sefrac`, a user-defined parameter, controls the stiffness of the mechanisms (Algorithm 1), `penal` (Eq. 12) denotes the penalty parameter of the SIMP scheme, which is set equal to 3, `kss` represents work-piece stiffness at the output location, and `rmin` is the filter radius. `etaf` and `betaf` are related to the flow coefficient (Eq. 2) and drainage term (Eq. 5) and `lst` decides whether load sensitivities are regarded or not. `lst = 1` indicates that the load sensitivities are included, whereas `lst = 0` directs otherwise. `betamax` is the maximum  $\beta$  permitted/used for the Heaviside projection (Eq. 13). `delrbst` represents the  $\Delta\eta$  of the robust formulation. `maxit` is the maximum number of the MMA iteration set for the topology optimization process. Discretization and DOFs (in local format) schemes are depicted in Fig. 3. The former is in global numbering style (Fig. 3a), whereas a local numbering scheme is used to demonstrate DOFs for element  $i$  (Fig. 3b). Figure 4 displays the main steps of SoRoTop MATLAB code. Steps performed in function `ObjCnst_ObjCnst_Sens` are marked inside a blue rectangle (Fig. 4).

The code consists of the following subroutines (Fig. 4):

1. Material and flow parameters initialization
2. Finite element and non-design domain preparation
3. Pressure and structure BCs, DOFs, Lagrange multipliers
4. Filter preparation
5. MMA optimization preparation
6. MMA optimization loop
7. Plotting results with final pressure field
8. Plotting deformed profile
9. Analyses performing function: `ObjCnst_ObjCnst_Sens`

Next, we describe each subroutine in detail.

#### 4.1 PART 1: Material and flow parameters initialization (lines 2-7)

Lines 2-7 of the code provide material and flow parameters for the design problem. Young's modulus of the material  $E_1$  is indicated on line 3 by `E1`, and that for the void element is mentioned on line 4 by `Emin`. `E1 = 1` and `Emin = E1 × 1 × 10-6` are set. `nu` represents Poisson's ratio set to 0.3 (line 5). The flow coefficient of the void element  $K_v$  is indicated by `Kv`. As indicated in Sec. 2.1, `Kv = 1` is set on line 6. `epsf` denotes the flow contrast  $\epsilon$  (line 6). `epsf = 1 × 10-7` is taken, i.e., the flow coefficient of the element with  $\rho = 1$ ,  $K_s$  equals to  $1 × 10<sup>-7</sup>$ . The parameters  $r$  (line 6),  $\Delta s$  (line 6) and  $Ds$  (line 7) related to the drainage are denoted by `r`, `DeIs`, and `Ds`, respectively (Sec. 2.1). `r = 0.1` and `DeIs = 2` are set (line 6). `Kvs` indicates  $K_v - K_s = Kv(1 - epsf)$  (line 7).

#### 4.2 PART 2: Finite element and non-design domain preparation (lines 8-38)

Lines 8-38 present finite element, non-design domain, and output DOF preparation. Line 9 determines the total number of elements and nodes participating in the discretized domain by `nel` and `nno`. Lines 10-12 are the standard procedure for determining element DOFs (Andreassen et al., 2011; Kumar, 2023). `Udofs` provides element-wise DOFs, i.e.,  $i^{\text{th}}$  row of `Udofs` gives DOFs associated with element  $i$

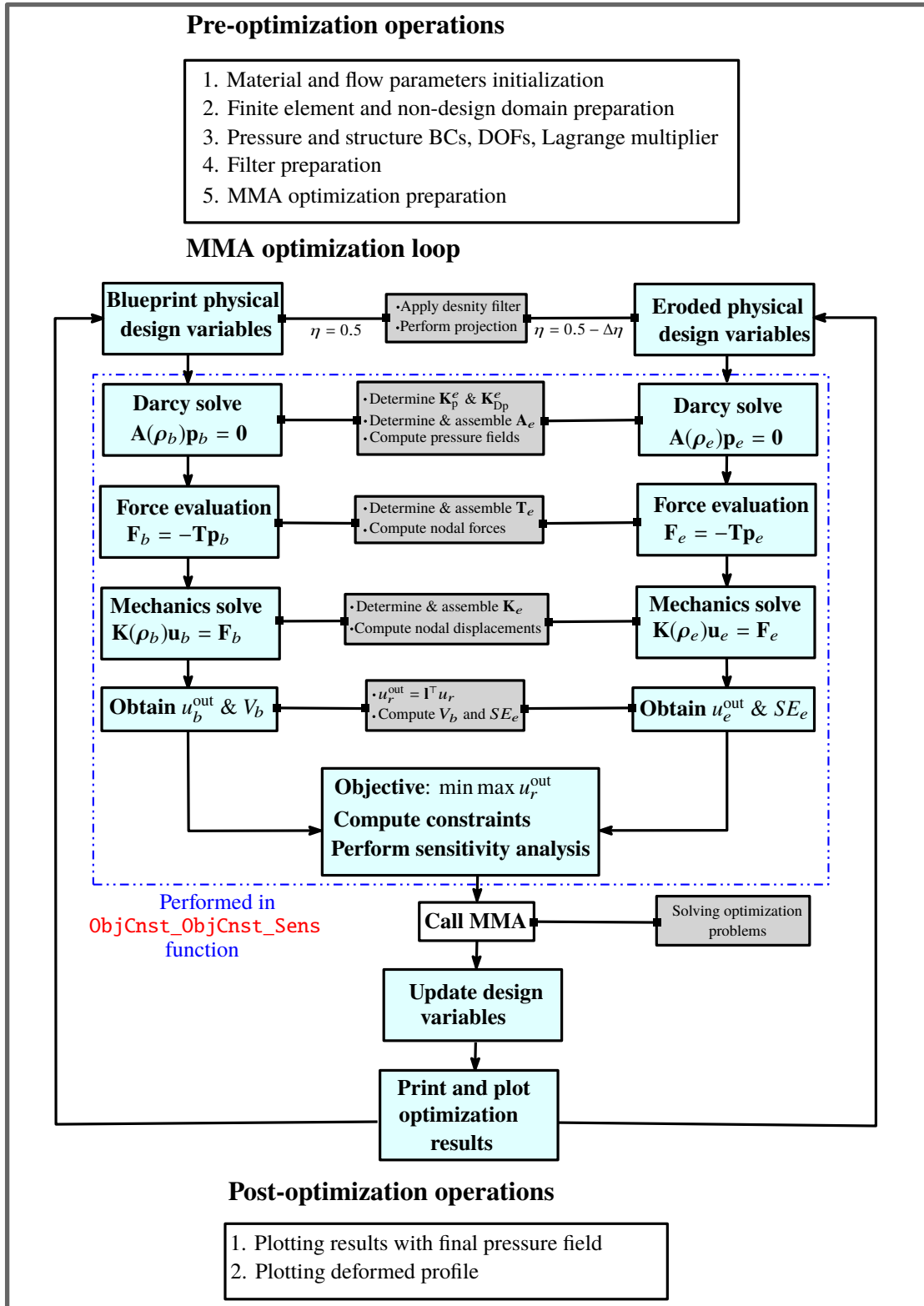


Figure 4: Flowchart for SoRoTop code

(line 12). Note that  $n^{\text{th}}$  node will have  $2n - 1$  and  $2n$  displacement DOFs in  $x$ - and  $y$ -directions, respectively and  $n$  pressure DOF (Fig. 3b). Nodes constituting left and right edges are determined on line 13 and are indicated via `Lnode` and `Rnode`, respectively. Likewise, on line 14, nodes constituting the bottom and top edges of the domain are found and are denoted via `Bnode` and `Tnode`, respectively. Line 15 determines different DOFs required for the finite element analysis. Matrices `Pdofs` and `allUdofs` are used to store DOFs associated with pressure and displacement fields, respectively.  $i^{\text{th}}$  columns of these matrices provide pressure and displacement DOFs of the nodes constituting element  $i$ . `allPdofs` indicates the entire pressure DOFs for the parameterized domain

We determine the element flow matrix due to Darcy law (`Kp`) on line 16, and that due to drainage term (`KDp`) on line 17 (Kumar, 2023). Matrices `Kp` and `KDp` are indicated via `Kp` and `KDp`, respectively, considering unit flow and drainage coefficients. Elemental transformation matrix (Eq. 10) is indicated by `Te` and is determined on line 18 (Kumar, 2023). Element stiffness matrix indicated by `Ke` is determined on line 23 per (Andreassen et al., 2011) for unit Young’s modulus. Matrices required to assemble `KDp`, `KDp`, `Te` and `Ke` to determine corresponding global matrices are determined on lines 24-29. Line 30 and line 32 provide function handles for the projection interpolation and its derivative, respectively. On line 34, a grid of elements is generated and recorded in `e1Nrs`. Using `e1Nrs`, the non-design solid region is determined on line 35 in vector `s1`. The elements associated with non-design solid and void regions are determined in matrices `NDS` and `NDV` on line 36, respectively. Union of `NDS` and `NDV` gives elements whose design variables do not change with optimization iterations. They are initialized using `deal` MATLAB function (line 36). Active design variables are determined and stored in `act` array on line 37. The DOF corresponding to the output node is noted in `opdof` on line 38.

### 4.3 PART 3: Pressure and structure BCs, DOFs, Lagrange multiplier (lines 39-49)

Lines 39-49 initialize parameters related to pressure and structure boundary conditions, pressure loads, fixed and free DOFs for pressure and displacement fields, Lagrange multipliers for the adjoint sensitivity calculation, and displacement and pressure vectors.

Vector `PF` indicates `p` field (Eq. 7), which is initialized on line 40. Scalar `Pin` stores the applied pressure load value (line 40). Line 41 modifies `PF` per given pressure loading conditions. Array `fixedPdofs` gives nodes corresponding to given pressure conditions (line 43). Free DOFs for the pressure load are determined on line 43 and are recorded in array `freePdofs`. Matrix `pfixeddofsv` gives fixed pressure DOFs in the first column and corresponding values in the second column. Fixed displacement DOFs are indicated on line 46 by array `fixedUdofs`. Line 46 evaluates the free displacement DOFs using `setdiff` MATLAB function with inputs vectors `allUdofs` and `fixedUdofs`. Lines 47-48 initialize vectors `L`, `U`, `lam1`, `lam2` and `mu2`. `L` represents vector  $l$  (Eq. 18), `U` is the global displacement vector  $u$  (Eq. 18), `lam1` and `lam2` are used to determine the objective sensitivity (Eq. 21), whereas for determining  $\mu_2$  constraint (eq. 18), Lagrange multiplier `mu2` is used in the function `Obj_ObjSens`. Vector `L` is modified corresponding to the output deformation DOF on line 49.

### 4.4 PART 4: Filter preparation (lines 50-70)

The filter preparation is performed on lines 50-70 per (Andreassen et al., 2011). One can also directly use the `imfilter` MATLAB function for filtering operation as done in (Ferrari et al., 2021; Kumar, 2023). `Hs` (Eq. 16) is determined on line 70 and is stored in matrix `Hs`.

### 4.5 PART 5: MMA optimization preparation (lines 71-83)

Lines 71-83 prepare the required parameters for the MMA optimizer. We have used the default setting available in the MMA for the min – max (Eq. 18) optimization problems. The design vector `x` is

initialized on line 72 to zeros. It is updated per the given `volfrac`, determined NDS and NDV on line 73 for the active set of design variables. Parameters `nMMA` (line 74) and `mMMA` (line 75) are used to indicate the number of design variables and constraints, respectively, that MMA is going to handle for the given problem. `pMMA` indicates the number of objectives considered within the robust optimization formulation. Herein, we consider output deformation values of the blueprint and eroded designs, i.e., `pMMA = 2` is set on line 74. Likewise, `qMMA` provides the number of constraints applied. A volume and a strain energy constraints are applied on the blueprint and eroded designs, respectively, i.e., `qMMA = 2` (line 74). The active design variables will be used in the MMA, which are copied in vector `xMMA` on line 73. The filtered design vector is initialized on line 75 in `xTilde`. `mvLt` indicates the external move limit of the MMA, which is set to 0.1 (line 75). On line 76, minimum and maximum values of the design vector are initialized in vectors `xminvec` and `xmaxvec`, respectively. The lower and upper limits on the design vector are set in vectors `low` and `upp`, respectively, on line 77. The parameters `cMMA`, `dMMA` and `a0` of the MMA (Svanberg, 1987) are initialized on line 78. On line 79, parameter `aMMA` is defined. Optimization is an iterative process; the old design vectors one and two iterations ago are recorded in vectors `xold1` and `xold2`, respectively. These vectors are initialized on line 80. A scalar `loop` counts the MMA iterations. The MMA loop is repeated until a convergence parameter `change` is lower than a  $1 \times 10^{-4}$  or provided number of iterations (`maxit`) is reached. The sharpness parameter  $\beta$  of the projection function (Eq. 13) is denoted by `betap`. `betap`, `loop` and `change` are initialized on line 81 using `deal` MATLAB function. On line 82, steps  $\eta$  (Eq. 13) for the blueprint (`etai`) and eroded (`etae`) designs are set to 0.5 and  $0.5 + \text{delrbst}$ . A constant `constadd = 10000` is set and used on line 107 so that `fval` of the MMA shall not become negative during optimization.

#### 4.6 PART 6: MMA optimization loop (lines 84-120)

Optimization iteration is performed on lines 84-120 using the parameters and variables defined above. Optimization starts with `while` loop on line 85. The `while` loop gets terminated if `loop` equals the maximum number of permitted optimization iterations `maxit` and `change` gets a value lower than  $1 \times 10^{-4}$ . The optimization procedure is divided into eight major subparts detailed below.

##### 4.6.1 PART 6.1: Compute blueprint and eroded physical design variables (lines 87-90)

Active filtered design variables `xTilde(act)` are assigned per `xMMA` on line 88, which is filtered using `Hs` (evaluated on line 70). Further, using vectors NDS and NDV, the filter vector `xTilde` is updated. Physical design vectors for the blueprint and eroded designs are represented via `xphysb` and `xphyse`, respectively. They are determined using the function handle `IFprj` with inputs `{xTilde, etab, betap}` and `{xTilde, etae, betap}` respectively. They are updated using vectors NDS and NDV.

##### 4.6.2 PART 6.2: Performing blueprint design analysis using `ObjCnst_ObjCnst_Sens` function (lines 91-93)

`ObjCnst_ObjCnst_Sens` function is called with `xphysb` as one of the input variables to perform analysis for the blueprint design. We record the required output of `Obj_ObjSens`. The output deformation and volume of the blueprint design are recorded in `objb` and `volb` (line 92). Blueprint objective and volume constraint sensitivities are noted in `objsensb` and `volsensb`, respectively. We also note the blueprint design displacement field, nodal forces, and pressure field in `Ub`, `Fb`, and `PFb`, respectively.

#### 4.6.3 PART 6.3: Performing eroded design analysis using `ObjCnst_ObjCnst_Sens` function (lines 94–96)

Similar to the blueprint design analysis, we call `ObjCnst_ObjCnst_Sens` function for eroded design but with `xphyse` as one of the physical input variables. The objective and strain energy are recorded in `obje` and `SEe`, and their sensitivities are noted in `objsense` and `SEsense`, respectively.

#### 4.6.4 PART 6.4: Filtering and projecting sensitivities of objectives and constraints (lines 97–101)

Sensitivities of obtained objective (`objsensb`, `objsense`) and constraints (`volsensb`, `SEsense`) are filtered and projected using `Hs` and `dIFprj`. `{xphysb, etab, betap}` and `{xphyse, etae, betap}` are respectively used as input variables to `dIFprj` for the blueprint and eroded designs.

#### 4.6.5 PART 6.5: Stacking constraints and their sensitivities (lines 102–105)

The current volume of the blueprint design and strain energy of the eroded design are stacked in `constr` on line 103. `constrsens` is used to stack sensitivities of the volume and strain energy constraints on line 104. These are performed to suit the requirements of the MMA. `normf` (line 105) normalizes objectives and sensitivities.

#### 4.6.6 PART 6.6: Setting and calling MMA optimizer (lines 106–111)

This section calls the `mmasub` function of the MMA optimizer on line 111 to solve the min – max optimization problem (Eq. 18). The default setting is used, wherein objectives and constraints are treated as constraints (Svanberg, 2007). The reader can refer to Svanberg (2007) for a detailed description of implementing min – max optimization problem using the MMA (Svanberg, 1987). `fval` is determined on line 107, wherein `constadd` is used to avoid getting negative entries for `fval` during optimization. `dfdx` is determined on line 108 using the objectives' and constraints' derivatives. On line 109, `xminvec` and `xmaxvec` are updated using the move limit.

#### 4.6.7 PART 6.7: Updating MMA/design variables and projection parameter $\beta$ (lines 112–116)

This part of the code updates the design variable vector `xMMA` using the solution obtained from the MMA on line 115. The vectors `xold1` and `xold2` are updated on line 113. The new solution of the MMA is recorded in `xnew` on line 113. `change` is determined on line 114 using the new and previous design variables.  $\beta$  (`betap`) of the projection filter (Eq. 13) is updated on line 116 at every 25th MMA iterations until it reaches the assigned maximum value `betamax`.

#### 4.6.8 PART 6.8: Print and plot the results (lines 117–120)

This part of the code print some important values (`loop`, `fval(1)`, i.e., `objb`, `fval(2)`, i.e., `obje`, `volb` using `mean(xphysb)`, and `change` of the optimization. Finally, the optimization evolution is plotted on line 119 using `colormap` and `imagesc` MATLAB functions. Next we describe post-optimization operations and `ObjCnst_ObjCnst_Sens` function.

## 4.7 Post-optimization operations

We perform two operations after optimization ends. Firstly, the optimized result is plotted with the final pressure field **PE**, described on lines 121-138 (PART 7). Nodal information is recorded on line 123 in matrix **node**. Each row of **node** has three entries, i.e.,  $i^{\text{th}}$  row indicates node  $i$  (first entry) with its  $x$ - (2nd entry) and  $y$ - (third entry) coordinates. Likewise, matrix **elem** contains element information with element number and its nodes. Matrices **X** (line 125) and **Y** (line 125) contain the  $x$ - and  $y$ -coordinates of nodes in element-wise sense. Matrix **Y1** is defined for plotting symmetric results. On line 127, the final pressure field (nodal pressure) is converted to elemental pressure loads and are stored in vector **elemP**. Lines 128-129 are used to plot the full optimized results using **patch** MATLAB function, wherein **X**, **Y**, **Y1** and **xphysb** quantities are used. Lines 130-138 plot the final pressure field using **patch** MATLAB function.

Secondly, the scaled-deformed profile is plotted on lines 139-155 (PART 8). The deformed nodal coordinates are stored in **xn** using **node** and **Ub** information (lines 141-144). **Xn** and **Yn** are determined using **xn**, they stored the  $x$ - and  $y$ -nodal coordinates in matrix form. Matrix **Yn1** (line 144) provides  $y$ -coordinates for symmetry half design. Finally, lines 147-155 plots the deformed profile using **patch** MATLAB function.

## 4.8 PART 9: ObjCnst\_ObjCnst\_Sens function

This function is written to perform FEM analyses pertaining to pressure field, objective and constraints evaluation, and derivative of objective and constraints determination. The function is called twice in the MMA optimization loop (Sec. 4.6) for the blueprint and eroded designs analyses. The function is provided with the code on lines 156-199 as

---

```
function [obj, objsens, vol, volsens, SEc, SEsens, U, F, PF] = ObjCnst_ObjCnst_Sens(xphys, nel,
    E1, Emin, penal, Kv, kvs, epsf, Ds, etaf, betaf, Udofs, freeUdofs, Pdofs, fixeddofsv,
    fixedPdofs, freePdofs, iP, jP, iT, jT, iK, jK, Kp, KDp, Te, ke, outputdof, kss, loop, IFprj, dIFprj
    , L, U, lam1, lam2, mu2, lst, volfrac, sefrac)
```

---

whose input and output variables are explained above (in subroutines 1-5 of SoRoTop code). We provide a detailed description function below that contains six subparts.

The first (lines 159-167) subpart provides the pressure field **PF**, i.e., solves Darcy law (Eq. 4). The flow coefficient **K** (Eq. 2) is indicated by **Kc** on line 160, which is determined using **Kv** (line 6), **epsf** (line 6) and **IFprj** (line 30). The drainage coefficient **D** (Eq. 5) is denoted by **Dc** on line 161. **Dc** is determined using **Ds** (line 7) and **IFprj** (line 30). The elemental flow matrices of all elements are recorded as a vector form in **Ae** on line 162. **Ae** is evaluated using **reshape** MATLAB function with **Kp** (line 16), **KDp** (line 17), **Kc** (line 160), **Dc** (line 161) and **nel**. Using **Ae**, **iP** (line 24) and **jP** (line 25) the global flow matrix **A** (Eq. 7) for the Darcy law with drainage term is evaluated on line 163 and recorded in **AG**. Using the free DOFs of pressure field, i.e., **freePdofs** (line 43), the corresponding flow matrix is determined on line 164 and recorded in **Aff**. We decompose **Aff** on line 165 using **decomposition** MATLAB function and recorded in **dAff\_ld1**. The pressure field **P** (Eq. 7) is determined on line 166 as per Eq. 8 and stored in **PF**. Finally, **PF** is updated on line 167 using the given pressure load stored in **fixeddofsv** (line 44).

The second (lines 168-177) subpart gives consistent global nodal load **F** (Eq. 10) and displacement (Eq. 18) vectors. On line 169, the element transformation matrix **T<sub>e</sub>** (Eq. 10) is written in a vector form in **Ts**. Using the matrices **iT** (line 26) and **jT** (line 27), we find the global transformation matrix **T** (Eq. 11) on line 170 and record in **TG**. **F** (Eq. 11) is determined on line 171 using matrix **TG** and vector **PF**. Young's modulus interpolation is performed on line 172 in vector **E**. The  $i^{\text{th}}$  entry of **E** provides Young's modulus of element  $i$ . The element stiffness matrices in a vector form using **Ke**, **E** and **nel** are arranged in **kss** on line 173. The global stiffness matrix **K** is evaluated on line 174 and is stored in **KG**. Matrix



KG is updated corresponding to the output degree of freedom `opdof` using the workpiece stiffness `kss`. On line 176, the global stiffness matrix is decomposed using `decomposition` MATLAB function with the Cholesky scheme. `U` is determined on line 177. In the third part (lines 178-179), the objective of the mechanism is determined using vectors `L` and `U`.

The fourth (lines 180-187) subpart provides the objective sensitivities per Sec. 3.2. `lam1` and `lam2` indicate  $\lambda_1$  (Eq. 21) and  $\lambda_2$  (Eq. 21), respectively. They are determined on line 181 and line 182, respectively. `objst1` determines the first part of the objective sensitivities (Eq. 24). Lines 184-186 evaluate the second part (Eq. 24), i.e., the load sensitivities. `dC1k` (line 184) and `dC1d` (line 185) determine the Darcy law and drainage parts, respectively, of the load sensitivities. On line 186, vector `objst2` records the load sensitivity terms. `objsens` stores the objective sensitivities on line 187. The fifth part determines the volume constraint `vol` (line 189) and its sensitivities `volsens` with respect to the design variables on line 190.

The last (line 191-199) subpart determines the strain energy sensitivities per Sec. 3.2. On line 192, the permitted strain energy `SE_perm` is determined using `sefrac` and strain energy determined at `loop = 1`. `SE_perm` is also saved and loaded on line 192. The strain energy constraint `SEc` (Eq. 23) and its sensitivities are determined on line 193 and line 199, respectively. `SET1` records the first part of the constraint sensitivities (Eq. 23), whereas `SET2` (Eq. 23) stores the second part of the sensitivities. `mu1` is the Lagrange multiplier needed to determine `SET2`. On line 196 and line 197, `dSEk`, the flow part of the sensitivities, and `dSEd`, the drainage part of the sensitivities, are determined. Finally, the strain energy sensitivities are determined on line 199 and stored in vector `SEsens`. Next, we present numerical results and discussions.

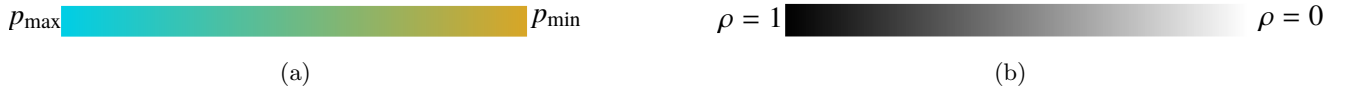


Figure 5: Colorbar schemes for the pressure and material fields are shown in (a) and (b), respectively.  $P_{\max} = 1$  bar and  $p_{\min} = 0$  bar.

## 5 Results and discussions

This section provides optimized pneumatically activated soft mechanisms using the presented code and extensions. The employed colorbar schemes for depicting the optimized material and pressure fields are shown in Fig. 5.

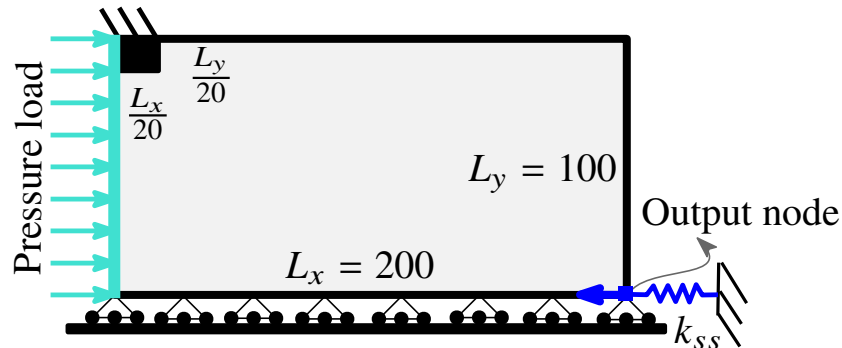


Figure 6: Inverter design domain

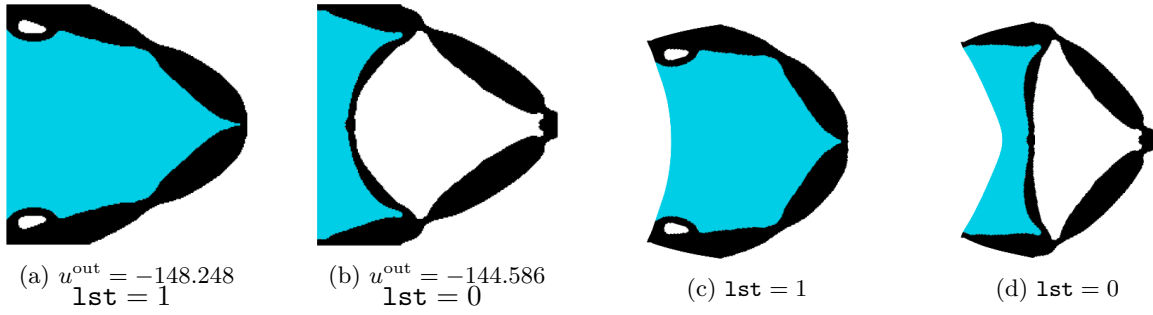


Figure 7: Pneumatically actuated optimized soft inverter mechanisms with (a)  $l_{1st} = 1$  and (b)  $l_{1st} = 0$ . Pneumatically actuated optimized soft inverter mechanisms in deformed configurations with (c)  $l_{1st} = 1$  and (d)  $l_{1st} = 0$ .

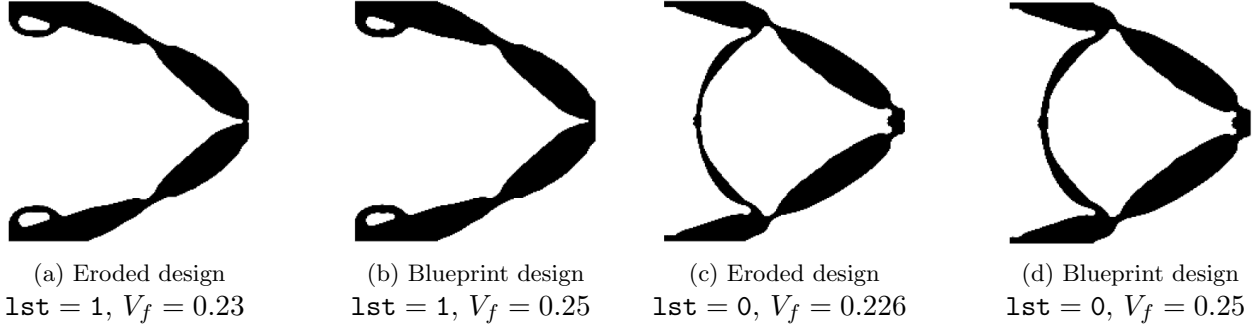


Figure 8: The eroded and blueprint (intermediate) optimized designs for the soft pneumatic inverters obtained with  $l_{1st} = 1$  and  $l_{1st} = 0$ .  $V_f$  indicates the final volume fraction.

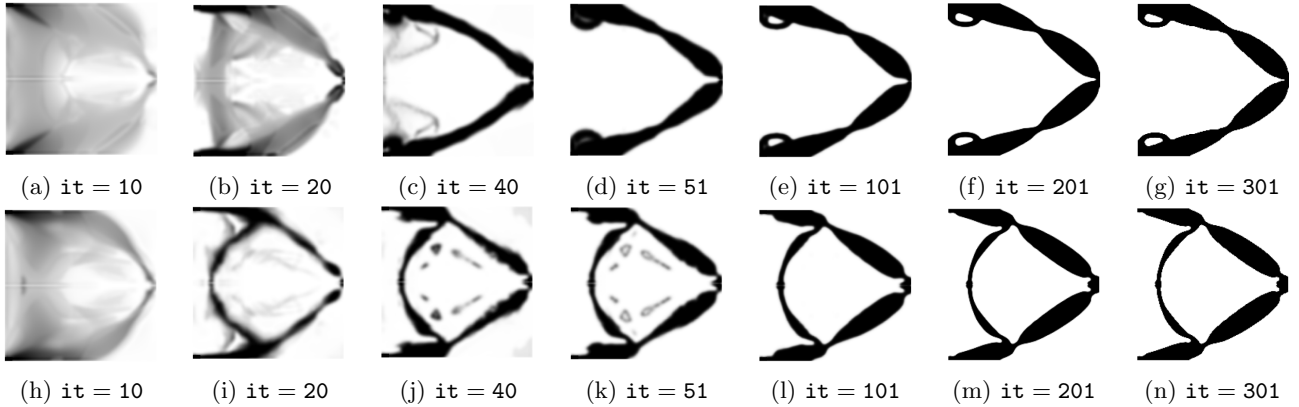


Figure 9: Intermediate results for the soft pneumatic inverter. (a) - (g) : Obtained with  $l_{1st} = 1$ . (h) - (n) : Obtained with  $l_{1st} = 0$ .  $it$  indicates the optimization iteration number.

## 5.1 Soft pneumatic inverter

Herein, soft pneumatic inverters are designed. Such mechanisms in 2D are reported in de Souza and Silva (2020); Kumar et al. (2020); Kumar and Langelaar (2022); Lu and Tong (2021); Kumar and Saxena (2022); Moscatelli et al. (2023), whereas Kumar and Langelaar (2021) also report a 3D pneumatic-actuated inverter mechanism. The provided code, SoRoTop, has the default setting for designing a soft inverter mechanism. The half symmetric design domain  $L_x \times L_y = 200 \times 100$  for the soft pneumatic inverter and its pressure and displacement boundary conditions are depicted in Fig. 6. The pressure/pneumatic load is applied on the left edge toward the  $+x$  direction, and the output node depicted in the figure is desired to move toward the  $-x$  direction. The top corner of the domain is fixed. A non-design solid domain of dimension  $\frac{L_x}{20} \times \frac{L_y}{20}$  exists as shown the figure. The symmetric boundary condition is also depicted (Fig. 6). One calls SoRoTop in the MATLAB command windows as

with `nelx` = 200, `nely` = 100, `volfrac` = 0.25, `sefrac` = 0.95, `penal` = 3, `rmin` = 4.8, `kss` = 1; `etaf` = 0.1, `betaf` = 8, `lst` = 1, `betamax` = 128, `delrbst` = 0.15 and `maxit` = 400. As `lst` = 1, i.e., the load sensitivities are included in the optimization.

The obtained symmetric result is transferred into a full design and is displayed in Fig. 7a. The corresponding deformed profile (scaled) is depicted in Fig. 7c.  $u^{\text{out}} = -148.248$  is obtained, i.e., the determined output deformation of the soft pneumatic inverter is in the desired direction.

We now use `lst` = 0 while keeping all the input variables of SoRoTop as above to demonstrate the effects of the load sensitivities on the optimized soft pneumatic inverter. With `lst` = 0, the optimized design and corresponding deformed profiles are shown in Fig. 7b and Fig. 7d, respectively.  $u^{\text{out}} = -144.586$  is obtained in the desired direction. The topology of the optimized design obtained with `lst` = 0 (Fig. 7b) is different than achieved with `lst` = 1 (Fig. 7a). The latter has a relatively bigger pressurized region than that of the former. Considering load sensitivities is physically right, it affects the topology of the optimized designs. The current observation aligns with that noticed in Kumar (2023) with TOPress MATLAB code for optimizing pressure loadbearing structures. The deformed profiles (scaled) are depicted in Fig. 7c and Fig. 7d with `lst` = 1 and `lst` = 0, respectively. The obtained output displacements of the optimized mechanisms are in the desired direction, i.e., in the negative  $x$ -direction. Fig. 8 depicts the eroded and blueprint soft pneumatic inverter optimized designs. The eroded designs contain relatively thinner members than the blueprint designs (Fig. 8). Fig. 9 shows some of the intermediate results for the blueprint designs with `lst` = 1 and `lst` = 0. The objective and volume fraction convergence plots are shown in Fig. 10. Steps in the plots appear due to change in the projection parameter  $\beta$ . The plots have a converging nature. Next, we present a study with different `delrbst` with and without load sensitivity terms to understand their effects on the optimized designs.

We consider `delrbst` = 0.10, and 0.01 with `lst` = 0, `lst` = 1 and the same input variables used above. Note `delrbst` with the filter radius decides the minimum length scale of the designs (Kumar and Langelaar, 2022; Fernández et al., 2020). Lower `delrbst` indicates that the minimum length scale of the blueprint and eroded designs are close. We call SoRoTop with the above `delrbst` values, `lst` = 1 or `lst` = 0 and with the above parameters. The optimized results are shown in Fig. 11. One can note that `lst` influences the optimized designs as noted above and also in Kumar (2023). With `lst` = 0, the optimized designs (Fig. 11b and Fig. 11d) contain intermediate arch connections—that restrict the full development of the pressure chambers. However, with `lst` = 1, unnecessary intermediate arch appendages are not obtained with the same parameters. Based on the numerical results, neglecting load sensitivities in penultimate load cases may not be the right idea. We use `lst` = 1 for soft pneumatic actuators designed below.

## 5.2 Soft pneumatic gripper

Soft pneumatic grippers are typically designed for applications that require gripping actions, e.g., gripping fruits, vegetables, eggs, pick and place items, etc. Considering the design-dependent characteristics of the load, 2D soft pneumatic grippers are designed in Kumar et al. (2020); Kumar and Langelaar (2022); Kumar and Saxena (2022); Lu and Tong (2021), whereas Refs. Panganiban et al. (2010); Kumar and Langelaar (2021); Pinskiar et al. (2023) design 3D soft grippers.

We modify SoRoTop code to design a soft pneumatic gripper herein. The half-symmetric design domain is displayed in Fig. 12. The pressure and displacement boundary conditions are applied as shown in Fig. 12. The pressure load is applied on the left edge and gripping action is desired at the right edge. Gripping jaw with dimension  $\frac{L_x}{5} \times \frac{L_y}{20}$  exists. To facilitate an object to be placed, a void region of dimension  $\frac{L_x}{5} \times \frac{L_y}{5}$  exists at the right/bottom edge. A solid non-design domain with dimension  $\frac{L_x}{20} \times \frac{L_y}{20}$

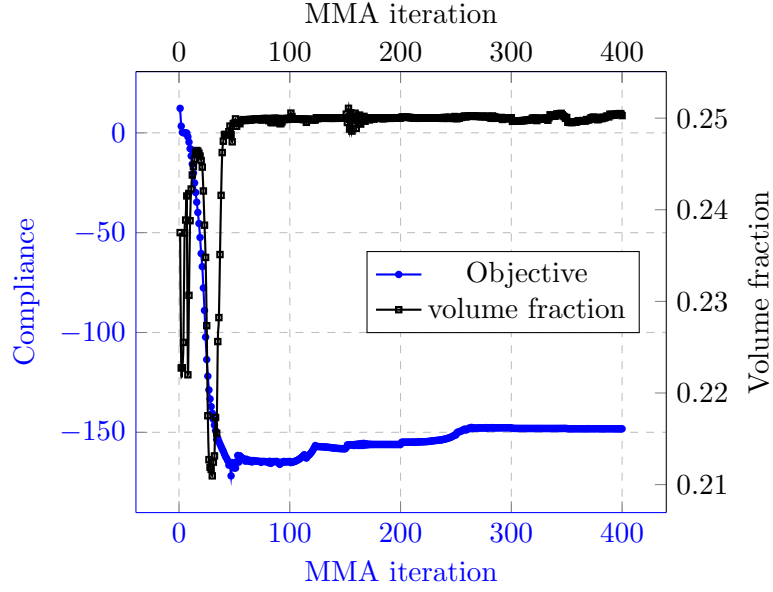


Figure 10: Objective and volume fraction convergence plots for the blueprint soft pneumatic inverter

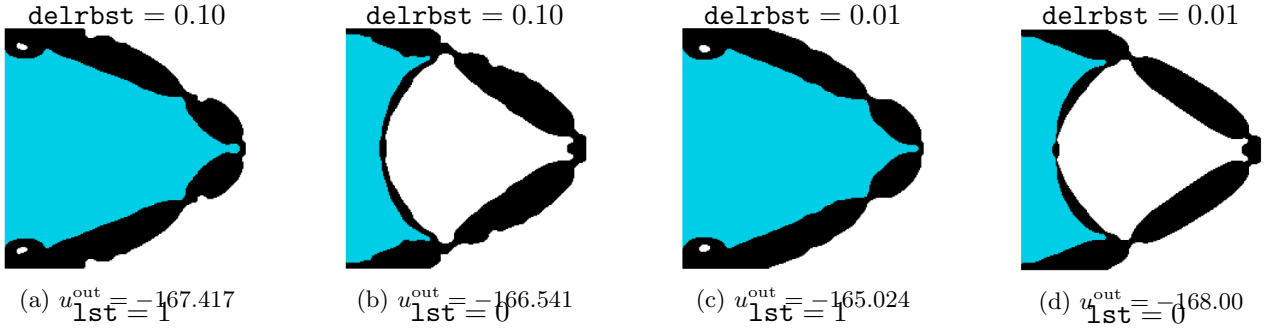


Figure 11: Optimized soft pneumatic inverters for different  $\Delta\eta$  with  $lst = 1$  and  $lst = 0$ .

also exists near the top left edge. One can modify the dimensions of the jaw and the void regions as per their requirement. The following modifications in SoRoTop are done for designing soft pneumatic gripper: Lines 34-38 are replaced by

---

```

elNrs = reshape(1:nel,nely,nelx); % element grid
s1=elNrs(1:nely/20,1:nelx/20); % Elem with rho =1
s2=elNrs(3*nely/4:4*nely/5,4*nelx/5:nelx); % Elem with rho =1
v1=elNrs(4*nely/5:nely,4*nelx/5:nelx); % Elem with rho =0
s = union (s1,s2); % Total elem with rho =1
[NDS, NDV ] = deal( s, v1 );
act = setdiff((1 : nel)', union( NDS, NDV )); %active set
opelem = elNrs(3*nely/4,nelx); % finding the output element
opnode = Pdofs(opelem,2); % finding the output node
opdof = 2*opnode; % output degree of freedom

```

---

other parts remain as it. With above modification, SoRoTop is called as

---

```

SoRoTop(200,100,0.30,0.90,3,5.6,1,0.1,10,1st,128,0.10,400)

```

---

with  $nelx = 200$ ,  $nely = 100$ ,  $volfrac = 0.30$ ,  $sefrac = 0.90$ ,  $penal = 3$ ,  $rmin = 5.6$ ,  $kss = 1$ ;  $etaf = 0.1$ ,  $betaf = 10$ ,  $lst = 1/0$ ,  $betamax = 128$ ,  $delrbst = 0.10$  and  $maxit = 400$ . The optimized results with  $lst = 1$  and  $lst = 0$  are shown in Fig. 13a and Fig. 13b, respectively. One again notes that the topology of the optimized designs with  $lst = 1$  and  $lst = 0$  are different. In the former case, a large part of the mechanism is made of a pressure chamber, whereas in the latter case, the size of the pressure chamber is relatively smaller. The output displacements of these gripper

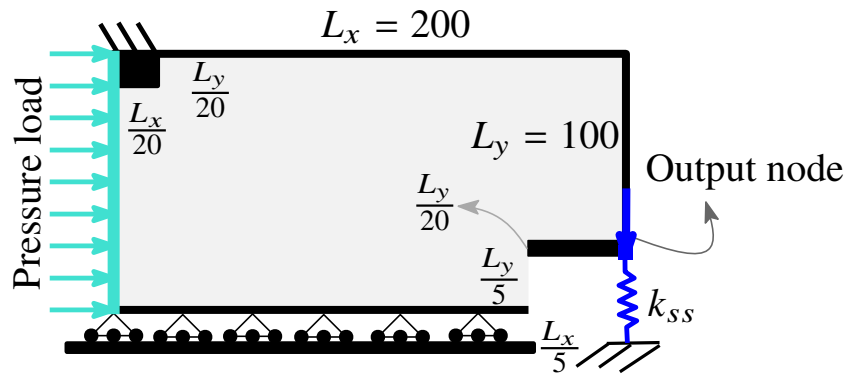


Figure 12: Gripper design domain

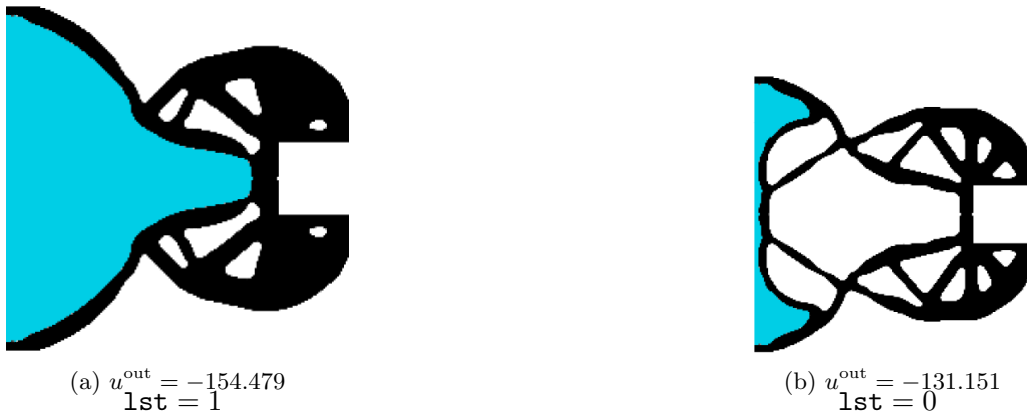


Figure 13: Pneumatically actuated soft gripper mechanisms

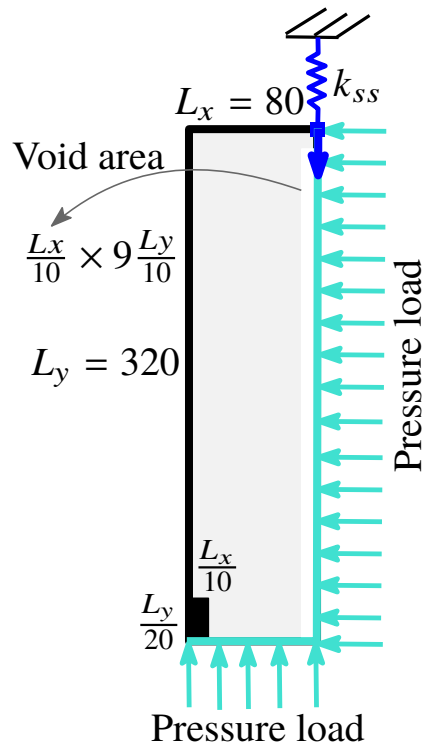


Figure 14: Soft pneumatic bending actuator design domain

mechanisms are in the desired direction, in that the soft mechanism obtained with  $1st = 1$  performs relatively better than that with  $1st = 0$ .

### 5.3 Soft pneumatic bending actuator

Herein, SoRoTop is modified to design a member of the pneumatic networks (PneuNets) mentioned in Lu and Tong (2022). The PneuNet is designed to achieve a bending motion. The symmetric-half design domain of a member is shown in Fig. 14. The pressure and displacement boundary conditions are also shown in the figure. It is desired that the output node upon pneumatic actuation should move down as depicted in Fig. 14. The non-design solid domain with dimension  $\frac{Lx}{10} \times \frac{Ly}{20}$  and non-design void domain of size  $\frac{Lx}{10} \times 9\frac{Ly}{10}$  exist.

The following modification in SoRoTop code is performed for designing this soft actuator:

Lines 34-38 are replaced by

---

```
e1Nrs = reshape(1:nel,nely,nelx); % element grid
s1 = e1Nrs(19*nely/20:nely,1:nelx/10); % Elem with rho =1
v1 = e1Nrs(nely/10:nely,9*nelx/10:nelx); % Elem with rho =0
[NDS, NDV ] = deal( s1, v1 );
act = setdiff((1 : nel)', union( NDS, NDV )); %active set
opdof = 2*Tnode(end); % output degree of freedom
```

---

Line 41 is modified for applying the pressure load boundary condition as

---

```
PF([Lnode, Tnode]) = 0; PF([Rnode, Bnode]) = Pin; % applying pressure load
```

---

and line 45 is changed for applying the displacement boundary condition as

---

```
fixedUdofs = [2*Lnode(end:-1:19*nely/20+1)-1 2*Lnode(end:-1:19*nely/20+1) 2*Rnode-1];
%fixed displ.
```

---

With the above modifications, SoRoTop code is called as

---

```
SoRoTop(80,320,0.2,0.90,3,7.6,1,0.1,10,1,128,0.1,400)
```

---

with  $nelx = 80$ ,  $nely = 320$ ,  $volfrac = 0.20$ ,  $sefrac = 0.90$ ,  $penal = 3$ ,  $rmin = 7.6$ ,  $kss = 1$ ;  $etaf = 0.1$ ,  $betaf = 10$ ,  $lst = 1$ ,  $betamax = 128$ ,  $delrbst = 0.10$  and  $maxit = 400$ . As the design domain is symmetric about  $y$ -axis. In the plotting subroutines (Sec. 4.7), line 126, line 133 and line 136 are changed to

---

```
X1 = 2*max(node(:,2))-reshape(node(elem(:,2:5)',2),4,nel); % for x-symmetry
patch(X1(:,i), Y(:,i), [1-elemP(i)], 'FaceColor', [0 0.8078 0.90], 'EdgeColor', 'none')
patch(X1(:,i), Y(:,i), [1-elemP(i)], 'FaceColor', 'w', 'EdgeColor', 'none')
```

---

respectively. Likewise, line 144, line 150 and line 153 are modified to

---

```
Xn1 = 2*max(node(:,2))-reshape(xn(elem(:,[2:5]'),2),4,nel); % for symmetry about x-axis
patch(Xn1(:,i), Yn(:,i), [1-elemP(i)], 'FaceColor', [0 0.8078 0.90], 'EdgeColor', 'none')
patch(Xn1(:,i), Yn(:,i), [1-elemP(i)], 'FaceColor', 'w', 'EdgeColor', 'none')
```

---

respectively.

Figure 15a display the full optimized result with the final pressure field. The optimized design (Fig. 15a) and its deformation profile (Fig. 15b) resemble that obtained in Lu and Tong (2022). Therefore, the performance of the PneuNets made via the optimized result shown in Fig. 15a is expected as that of Lu and Tong (2022).

### 5.4 Centrally pressurized soft pneumatic actuator

Next, to demonstrate the additional capabilities of the presented code, we design a centrally pressurized soft pneumatic actuator. The design domain of the actuator is depicted in Fig. 16. The pressure load



Figure 15: Optimized soft pneumatic bending actuator. (a) Optimized design and (b) Scaled deformed design

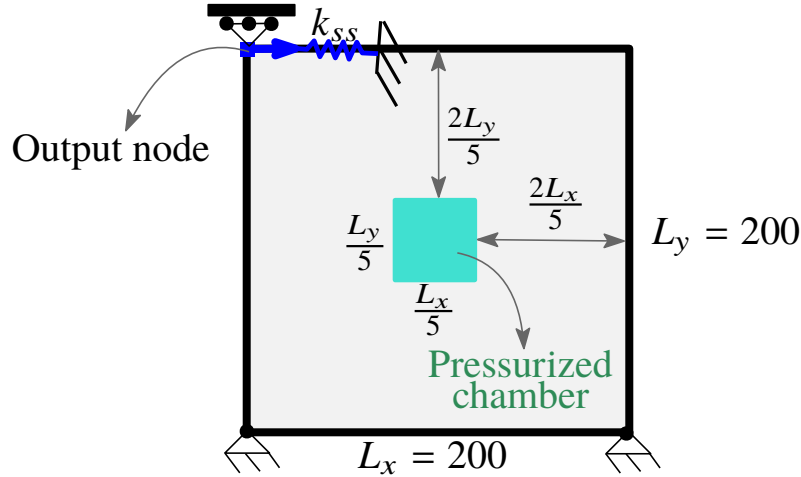


Figure 16: Centrally pressurized soft pneumatic actuator design domain

is applied in the central chamber having dimension  $\frac{L_x}{10} \times \frac{L_y}{10}$ , which is considered a void region. Edges of the domain are set at zero pressure level. The output location and the desired deformation are depicted in the figure. The left and right ends of the bottom edge are fixed (Fig. 16). The following modifications are done to optimize the centrally pressurized soft pneumatic actuator. Lines 35-36 are replaced by

---

```
v1 = e1Nrs(2*nely/5:3*nely/5,2*nelx/5:3*nelx/5);
[NDS, NDV ] = deal([], v1);
```

---

As the desired output deformation is in positive  $x$ -direction, the line 38 is replaced by

---

```
opdof = 2*Tnode(1)-1; % output degree of freedom
```

---

The pressure is applied on the central region (Fig. 16); thus, the nodes associated with the domain are determined and stored in vector `nodeV1`. A line is inserted after line 38 for `nodeV1` as

---

```
nodeV1 = unique(Pdofs(v,:)); % pressurized nodes
```

---

The given pressure load conditions are applied by altering line 41 to

---

```
PF([Lnode, Bnode, Tnode, Rnode]) = 0; PF(nodeV1) = Pin;
```

---

Line 45 is changed to apply the displacement boundary conditions as

---

```
fixedUdofs = [2*Bnode(1)-1 2*Bnode(1) 2*Bnode(end)-1 2*Bnode(end) 2*Tnode(1)]; %fixed displ.
```

---





Figure 17: Optimized centrally pressurized soft pneumatic actuator. (a) Optimized design and (b) Scaled deformed design

In addition to the above mentioned changes, we remove the symmetry plotting lines from PART 7 and PART 8. Finally, we call the code as

---

```
SoRoTop(200,200,0.25,0.9,3,6.6,1,0.1,10,1,128,0.05,400)
```

---

with `nelx = 200`, `nely = 200`, `volfrac = 0.25`, `sefrac = 0.90`, `penal = 3`, `rmin = 6.6`, `kss = 1`; `etaf = 0.1`, `betaf = 10`, `lst = 1`, `betamax = 128`, `delrbst = 00.1` and `maxit = 400`.

Figure 17a provides the optimized design for the centrally pressurized soft pneumatic actuator. The pressure chamber gets an arbitrary shape that helps achieve the desired deformation, as noted in the deformed profile shown in Fig. 17b.

Likewise, a user can optimize different pneumatically actuated soft robots by changing the displacement and pressure boundary conditions using SoRoTop. In addition, the code can readily be extended with different necessary constraints if needed.

## 6 Concluding remarks

This paper presents a MATLAB code, named SoRoTop, for designing soft pneumatic actuators using TO. Such actuators find various applications; however, it is a challenging and complex task to model the design-dependent nature of the pneumatic loads within a TO setting, as such loads change their direction, magnitude, and/or location with the optimization iterations. Thus, to ease newcomers' and students' learning paths toward designing soft pneumatic actuators, the code is developed per the method first introduced in Kumar et al. (2020). The code uses the robust formulation with eroded and blueprint designs to circumvent the appearance of single-node connections in the optimized mechanisms. SoRoTop is explained in detail and is extended to optimize different soft pneumatic actuators. The paper also demonstrates that load sensitivities have a significance impact on the optimized topology of these actuators. Hence, it is essential not to overlook them when conducting a TO.

The method proposed in Kumar et al. (2020) is employed to model the design-dependent pneumatic load. The flow and drainage terms are interpolated using the Heaviside functions. The obtained pressure field is converted to consistent nodal loads using a transformation matrix. The objective's and constraints' sensitivities are determined using the adjoint-variable method; thus, the load sensitivities. One can toggle load sensitivity terms to 1 or 0 using `lst` input parameter. The optimization is formulated as a min-max problem, involving both blueprint and eroded design descriptions. The method of moving asymptotes is employed for the optimization. Volume constraint is applied to the blueprint design, whereas a strain energy constraint is applied to the eroded design. A strain energy fraction parameter `sefrac` is introduced to apply the latter constraint which assists in attaining optimized

designs that can endure the applied load without sacrificing performance. Based on the results of the numerical experiments performed, we observe,  $\mathbf{sefrac} \in [0.80 \ 0.95]$  performs well, resulting in achievable, leak-proof optimized designs. One may also opt to reduce  $\mathbf{sefrac}$  in a specific problem to ensure a leak-proof design. Objective and volume fraction plots reveal that they have a converging nature. The volume fraction remains active and satisfied at the end of the optimization.

SoRoTop is provided in Appendix A, and it is extended to optimize different soft pneumatic actuators. The code is structured into pre-optimization, MMA optimization, and post-optimization operations, and each operation is described in detail. The design of four pneumatically activated soft robots demonstrates the efficacy and robustness of code. Integrating the code with nonlinear mechanics forms a complex and exciting future direction. We believe that newcomers, students, and the soft robotics research community will take advantage of the provided code, and they will utilize and extend the code to generate soft pneumatic actuators for different applications.

## Acknowledgments

The author thanks Matthijs Langelaar and Ole Sigmund for discussions on the method in the past, Krister Svanberg (krille@math.kth.se) for providing MATLAB codes of the MMA optimizer, and Indian Institute of Technology Hyderabad for the support under the seed grant with project file number SG/IITH/F297/2022-23/SG-155.

## Declaration of Competing Interest

None.

## Appendix A The MATLAB code: SoRoTop

```

1 function SoRoTop(nelx,nely,volfrac,sefrac,penal,rmin,kss,etaf,betaf,lst,betamax,delrbst,maxit)
2 %% ---PART 1.-----MATERIAL AND FLOW PARAMETERS
3 E1 = 1;
4 Emin = E1*1e-6;
5 nu = 0.30;
6 [Kv,epsf,r,Dels] = deal(1,1e-7,0.1,2); % flow parameters
7 [Ds, Kvs]= deal((log(r)/Dels)^2*epsf,Kv*(1 - epsf)); % flow parameters
8 %% ---PART 2.-----FINITE ELEMENT and NON-DESIGN DOMAIN PREPARATION
9 [nel,nno] = deal(nelx*nely, (nelx+1)*(nely+1));
10 nodenrs = reshape(1:(1+nelx)*(1+nely),1+nely,1+nelx);
11 edofVec = reshape(2*nodenrs(1:end-1,1:end-1)+1,nelx*nely,1);
12 Udofs = repmat(edofVec,1,8)+repmat([0 1 2*nely+[2 3 0 1] -2 -1],nelx*nely,1);
13 [Lnode,Rnode]= deal(1:nely+1, (nno-nely):nno);
14 [Bnode,Tnode]= deal((nely+1):(nely+1):nno, 1:(nely+1):(nno-nely));
15 [Pdofs,allPdofs,allUdofs] = deal(Udofs(:,2:2:end)/2,1:nno,1:2*nno);
16 Kp = 1/6*[4 -1 -2 -1;-1 4 -1 -2;-2 -1 4 -1;-1 -2 -1 4]; % flow matrix: Darcy Law
17 KDp = 1/36*[4 2 1 2; 2 4 2 1; 1 2 4 2; 2 1 2 4]; % Drainage matrix
18 Te = 1/12*[-2 2 1 -1;-2 -1 1 2;-2 2 1 -1;-1 -2 2 1;-1 1 2 -2;-1 -2 2 1;-1 1 2 -2;-2 -1 1 2];
19 % transformation matrix
20 A11 = [12 3 -6 -3; 3 12 3 0; -6 3 12 -3; -3 0 -3 12];
21 A12 = [-6 -3 0 3; -3 -6 -3 -6; 0 -3 -6 3; 3 -6 3 -6];
22 B11 = [-4 3 -2 9; 3 -4 -9 4; -2 -9 -4 -3; 9 4 -3 -4];
23 B12 = [2 -3 4 -9;-3 2 9 -2; 4 9 2 3;-9 -2 3 2];
24 Ke = 1/(1-nu^2)/24*([A11 A12;A12' A11]+nu*[B11 B12;B12' B11]); %stiffness matrix
25 iP = reshape(kron(Pdofs,ones(4,1))',16*nel,1);
26 jP = reshape(kron(Pdofs,ones(1,4))',16*nel,1);
27 iT = reshape(kron(Udofs,ones(4,1))',32*nel,1);
28 jT = reshape(kron(Pdofs,ones(1,8))',32*nel,1);
29 iK = reshape(kron(Udofs,ones(8,1))',64*nel,1);
30 jK = reshape(kron(Udofs,ones(1,8))',64*nel,1);
31 IFprj=@(xv,etaf,betaf)((tanh(betaf*etaf) + tanh(betaf*(xv-etaf)))/... %projection
32 function
33 (tanh(betaf*etaf) + tanh(betaf*(1 - etaf))));
34 dIFprj=@(xv,etaf,betaf) betaf*(1-tanh(betaf*(xv-etaf)).^2)...
35 /(tanh(betaf*etaf)+tanh(betaf*(1-etaf))); % derivative of the projection
36 function
37 elNrs = reshape(1:nel,nely,nelx); % element grid
38 s1 = elNrs(1:nely/20,1:nelx/20); % Solid element or
39 element with rho =1
40 [NDS, NDV ] = deal( s1, [] );
41 act = setdiff((1 : nel)', union( NDS, NDV ));
42 op dof = 2*Bnode(end)-1;
43 %% ---PART 3.---PRESSURE & STRUCTURE B.C's, LOADs, DOFs, Lag. Multi.,sL
44 [PF, Pin] =deal(0.00001*ones(nno,1),1); %pressure-field preparation
45 PF([Tnode, Rnode]) = 0; PF(Lnode) = Pin; % applying pressure load
46 fixedPdofs = allPdofs(PF~=0.00001);
47 freePdofs = setdiff(allPdofs, fixedPdofs);
48 pfixeddofsv = [fixedPdofs' PF(fixedPdofs)]; % p-fixed and its value
49 fixedUdofs = [2*Tnode(1:nely/20)-1 2*Tnode(1:nely/20) 2*Bnode]; %fixed displ.
50 freeUdofs = setdiff(allUdofs, fixedUdofs);
51 [L,U,lam2] = deal(zeros(2*nno,1));
52 [lam1,mu1] = deal(zeros(nno,1)); %initialize lambda
53 [L(opdof)] = 1 ; % dummy load and spring constant
54 %% ---PART 4.-----FILTER PREPARATION
55 iH = ones(nelx*nely*(2*(ceil(rmin)-1)+1)^2,1);
56 jH = ones(size(iH));
57 sH = zeros(size(iH));
58 k = 0;
59 for i1 = 1:nelx
60 for j1 = 1:nely
61 e1 = (i1-1)*nely+j1;
62 for i2 = max(i1-(ceil(rmin)-1),1):min(i1+(ceil(rmin)-1),nelx)
63 for j2 = max(j1-(ceil(rmin)-1),1):min(j1+(ceil(rmin)-1),nely)
64 e2 = (i2-1)*nely+j2;
65 k = k+1;
66 iH(k) = e1;
67 jH(k) = e2;
68 sH(k) = max(0,rmin-sqrt((i1-i2)^2+(j1-j2)^2));
69 end
70 end
71 end

```

```

68 end
69 H = sparse(iH,jH,sH);
70 Hs = H./sum(H,2); % matrix of weights (filter)
71 %% _____PART 5_____ MMA OPTIMIZATION PREPARATION & INITIALIZATION
72 x = zeros(nel,1); % design variable
73 x(act) = (volfrac*(nel-length(NDV))-length(NDS) )/length(act); x(NDS) = 1;
74 [nMMA,pMMA,qMMA] = deal(length(act),2,2);
75 [mMMA,xMMA,xTilde,mvLt] = deal(pMMA+qMMA,x(act),x,0.1);
76 [xminvec,xmaxvec] = deal(zeros(nMMA,1),ones(nMMA,1)); %Min. & Max
77 [low, upp] = deal(xminvec,xmaxvec); % Low and Upp limits MMA
78 [cMMA,dMMA, a0] = deal(1000*ones(mMMA,1),zeros(mMMA,1),1);
79 aMMA = [ones(pMMA,1); zeros(qMMA,1)];
80 [xold1,xold2] = deal(xMMA);
81 [betap,loop, change] = deal(1,0,1);
82 [etab,etae] =deal(0.5,0.5+delrbst);
83 costadd = 10000;
84 %% _____PART 6_____ MMA OPTIMIZATION LOOP
85 while(loop<maxit && change>0.0001)
86 loop = loop + 1; % Updating the opt. iteration
87 %___PART 6.1_____Compute blueprint and eroded physical desing variables
88 xTilde(act) = xMMA; xTilde =Hs'*xTilde; xTilde(NDS)=1; xTilde(NDV)=0;
89 xphysb = IFprj(xTilde,etab,betap); xphysb(NDS)=1; xphysb(NDV)=0;
90 xphyse = IFprj(xTilde,etae,betap); xphyse(NDS)=1; xphyse(NDV)=0;
91 %___PART 6.2_____Performing blueprint design analysis using ObjObjSens function
92 [objjb, objjsensb,volb,volsensb, ~, ~,Ub,Fb,PFb] = ObjCnst_ObjCnst_Sens(xphysb,nel,E1,Emin,penal,
Kv,Kvs,epsf,Ds,etaf,betaf,Udofs,freeUdofs,
93 Pdofs,pfixeddofsv,fixedPdofs,freePdofs,iP,jP,iT,jT,iK,jK,Kp,KDp,Te,Ke,opdof,kss,loop,IFprj,
dIFprj,L,U,lam1,lam2,mu1,lst,volfrac,sefrac);
94 %___PART 6.3_____Performing eroded design analysis using ObjObjSens function
95 [objje, objjsense,~,~, SEe, SEsense,~,~,~] = ObjCnst_ObjCnst_Sens(xphyse,nel,E1, Emin,penal,Kv,
Kvs,epsf,Ds,etaf,betaf,Udofs,freeUdofs, ...
96 Pdofs,pfixeddofsv,fixedPdofs,freePdofs,iP,jP,iT,jT,iK,jK,Kp,KDp,Te,Ke,opdof,kss,loop,IFprj,
dIFprj,L,U,lam1,lam2,mu1,lst,volfrac,sefrac);
97 %___PART 6.4_____Filtering and projecting objective and constraints
sensitivities
98 objjsensb = Hs'*(objjsensb.*dIFprj(xphysb,etab,betap)); % blueprint sensitivity
99 objjsense = Hs'*(objjsense.*dIFprj(xphyse,etae,betap));
100 volsensb = Hs'*(volsensb.*dIFprj(xphysb,etab,betap));
101 SEsense = Hs'*(SEsense.*dIFprj(xphyse,etae,betap));
102 %___PART 6.5_____Stacking constraints and their sensitivities
103 constr =[volb SEe];
104 constrsens = [volsensb SEsense];
105 normf = 1;
106 %___PART 6.6_____SETTING and CALLING MMA OPTIMIZATION
107 fval = [costadd + objjb*normf,costadd + objje*normf,constr]';
108 dfdx = [objjsensb(act,:)*normf, objjsense(act,:)*normf, constrsens(act,:)']';
109 [xminvec, xmaxvec]= deal(max(0, xMMA - mvLt),min(1, xMMA + mvLt));
110 [xmma,~,~,~,~,~,~,~,low,upp] = mmasub(mMMA,nMMA,loop,xMMA,xminvec,xmaxvec,xold1,xold2, ...
111 0,0,0,fval,dfdx,0*dfdx,low,upp,a0,aMMA,cMMA,dMMA);
112 %___PART 6.7_____Updating_____
113 [xold2,xold1, xnew]= deal(xold1, xMMA,xmma);
114 change = max(abs(xnew-xMMA)); % Calculating change
115 xMMA = xnew;
116 if(mod(loop,50)==0 && betap<=betamax), betap= betap*2;end % beta updation
117 %___PART 6.8_____Printing and plotting results
118 fprintf(' It.:%5i Obji.:%11.4f Obje.:%11.4f Voli.:%7.3f ch.:%7.3f\n',loop,fval(1),fval(2),mean
(xphysb),change);
119 colormap(gray); imagesc(1-reshape(xphysb, nely, nelx));caxis([0 1]);axis equal off;drawnow;
120 end
121 %% _____PART 7_____plotting results with final pressure field_____
122 PFP = figure(2); set(PFP,'color','w'); axis equal off, hold on; colormap('gray');
123 node = [ (1:nno)' reshape(repmat(0:nelx,nely+1,1),nno,1) repmat(0:-1:-nely,1, nelx+1)']; %
nodal coordinates
124 elem(:,1) = (1:nel)'; elem(:,2:5) = Pdofs; % element and connectivity information
125 X = reshape(node(elem(:,2:5)')',2),4,nel); Y = reshape(node(elem(:,2:5)')',3),4,nel);
126 Y1 = 2*min(node(:,3))-reshape(node(elem(:,2:5)')',3),4,nel); % for x-symmetry
127 for i = 1:nel,elemP(i) = sum(PFb(elem(i,2:5)))/4/Pin;end
128 patch(X, Y, [1-xphysb],'EdgeColor','none');caxis([0 1]);
129 patch(X, Y1, [1-xphysb],'EdgeColor','none');caxis([0 1]);
130 for i = 1:nel
131 if (xphysb(i)<0.2 && elemP(i)>0.70)
132 patch(X(:,i), Y(:,i), [1-elemP(i)],'FaceColor',[0 0.8078 0.90],'EdgeColor','none')
133 patch(X(:,i), Y1(:,i), [1-elemP(i)],'FaceColor',[0 0.8078 0.90],'EdgeColor','none')
134 elseif (xphysb(i)<0.2 && elemP(i)<0.70)

```

```

135 patch(X(:,i), Y(:,i), [1-elemP(i)], 'FaceColor', 'w', 'EdgeColor', 'none')
136 patch(X(:,i), Y1(:,i), [1-elemP(i)], 'FaceColor', 'w', 'EdgeColor', 'none')
137 end
138 end
139 %% -----PART 8-----Plotting deformed profile-----
140 DFP = figure(3); set(DFP, 'color', 'w'); axis equal off, hold on; colormap(gray); caxis([0 1]);
141 xn= node; % defomed nodal position
142 xn(:,2) = node(:,2) + 0.0025*Ub(1:2:end); xn(:,3) = node(:,3) + 0.0025*Ub(2:2:end);
143 Xn = reshape(xn(elem(:, [2:5])'), 2, 4, nel); Yn = reshape(xn(elem(:, [2:5])'), 3, 4, nel);
144 Yn1 = 2*min(node(:,3))-reshape(xn(elem(:, [2:5])'), 3, 4, nel); % for symmetry about x-axis
145 patch(Xn, Yn, [1-xphysb], 'EdgeColor', 'none');
146 patch(Xn, Yn1, [1-xphysb], 'EdgeColor', 'none');
147 for i = 1:nel
148 if (xphysb(i)<0.2 && elemP(i)>0.70)
149 patch(Xn(:,i), Yn(:,i), [1-elemP(i)], 'FaceColor', [0 0.8078 0.90], 'EdgeColor', 'none');
150 patch(Xn(:,i), Yn1(:,i), [1-elemP(i)], 'FaceColor', [0 0.8078 0.90], 'EdgeColor', 'none');
151 elseif (xphysb(i)<0.2 && elemP(i)<0.70)
152 patch(Xn(:,i), Yn(:,i), [1-elemP(i)], 'FaceColor', 'w', 'EdgeColor', 'none');
153 patch(Xn(:,i), Yn1(:,i), [1-elemP(i)], 'FaceColor', 'w', 'EdgeColor', 'none');
154 end
155 end
156 %% -----PART 9----- Analyses function
157 function[obj, objsens, vol, volsens, SEc, SEsens, U, F, PF] = ObjCnst_ObjCnst_Sens(xphys, nel, E1, Emin,
penal, Kv, kvs, epsf, Ds, etaf, betaf, Udofs, ...
158 freeUdofs, Pdofs, pfixeddofsv, fixedPdofs, freePdofs, iP, jP, iT, jT, iK, jK, Kp, KDp, Te, Ke, opdof, kss, loop,
IFprj, dIFprj, L, U, lam1, lam2, mu1, lst, volfrac, sefrac)
159 % ___PATT 9.1-----SOLVING FLOW BALANCE EQUATION
160 Kc = Kv*(1-(1-epsf))*IFprj(xphys, etaf, betaf); %Flow coefficient
161 Dc = Ds*IFprj(xphys, etaf, betaf); %Drainage coefficient
162 Ae = reshape(Kp(:)*Kc' + KDp(:)*Dc', 16*nel, 1); %Elemental flow matrix in vector form
163 AG = (sparse(iP, jP, Ae) + sparse(iP, jP, Ae))/2; %Global flow matrix
164 Aff = AG(freePdofs, freePdofs); %AG for free pressure dofs
165 dAff_ldl = decomposition(Aff, 'ldl'); % Decomposing Aff matrix
166 PF(freePdofs, 1) = dAff_ldl\(-AG(freePdofs, fixedPdofs)*pfixeddofsv(:, 2));
167 PF(pfixeddofsv(:, 1), 1) = pfixeddofsv(:, 2); % Final P-field
168 %__PART 9.2_DETERMINING CONSISTENT NODAL LOADS and GLOBAL Disp. Vector
169 Ts = reshape(Te(:)*ones(1, nel), 32*nel, 1); %Elemental transformation matrix in vector
form
170 TG = sparse(iT, jT, Ts); %Global transformation matrix
171 F = -TG*PF; % Dertmining nodal forces
172 E = Emin + xphys.^penal*(E1 - Emin); %Material interpolation
173 Ks = reshape(Ke(:)*E', 64*nel, 1); %Elemental stiffness matrix in vector
form
174 KG = (sparse(iK, jK, Ks) + sparse(iK, jK, Ks))/2; %Global stiffnes matrix
175 KG(opdof, opdof) = KG(opdof, opdof) + kss; % adding the workpiece stiffness
176 dKG_chol = decomposition(KG(freeUdofs, freeUdofs), 'chol', 'lower'); % decomposed freedofs
stiffness
177 U(freeUdofs) = dKG_chol\F(freeUdofs); %Global Disp. Vect.
178 %__PART 9.3-----objective evaluation
179 obj = L'*U; % maximizing the output deformation
180 %__PART 9.4-----sensitivity analysis
181 lam2(freeUdofs) = -dKG_chol\L(freeUdofs);
182 lam1(freePdofs) = -(lam2(freeUdofs))*TG(freeUdofs, freePdofs)/dAff_ldl;
183 objsT1 = (E1 - Emin)*penal*xphys.^(penal - 1).*sum((lam2(Udofs)*Ke).*U(Udofs), 2);
184 dC1k = -dIFprj(xphys, etaf, betaf).* sum((lam1(Pdofs)*(kvs*Kp)) .* PF(Pdofs), 2);
185 dC1d = dIFprj(xphys, etaf, betaf).* sum((lam1(Pdofs)*(Ds*KDp)) .* PF(Pdofs), 2);
186 objsT2 = dC1k + dC1d;
187 objsens = (objsT1 + lst*objsT2); % final sensitivities
188 %__PART 9.5----volume sensitivities
189 vol = sum(xphys)/(nel*volfrac)-1;
190 volsens = 1/(volfrac*nel)*ones(nel, 1);
191 %___PART 9.6----Strain energy sensitivities
192 if(loop==1), SE_perm = sefrac*(0.5*U'*KG*U); save SE_perm SE_perm; end; load SE_perm
193 SEc = 0.5*U'*KG*U/SE_perm -1;
194 SET1 = -0.5*(E1 - Emin)*penal*xphys.^(penal - 1).*sum((U(Udofs))*Ke).*U(Udofs), 2);
195 mu1(freePdofs) = (U(freeUdofs))*TG(freeUdofs, freePdofs)/dAff_ldl;
196 dSEk = -dIFprj(xphys, etaf, betaf).* sum((mu1(Pdofs)*(kvs*Kp)) .* PF(Pdofs), 2);
197 dSEd = dIFprj(xphys, etaf, betaf).* sum((mu1(Pdofs)*(Ds*KDp)) .* PF(Pdofs), 2);
198 SET2 = dSEk + dSEd;
199 SEsens = (SET1 + SET2)/SE_perm;

%%%%%%%%%%%%%%%%%%%%%%%%%%%%%%%%%%%%%%%%%%%%%%%%%%%%%%%%%%%%%%%%%%%%%%%%%%%%%%
% SoRoTop is written for pedagogical purposes. A detailed description can be %
% found in the paper:"SoRoTop: a hitchhiker's guide to topology optimization %

```

```

%   MATLAB code for design-dependent pneumatic-driven soft robots" Optimization   %
%   and Engineering, 2023.                                                         %
%                                                                                   %
%   Code and its extensions are available online as supplementary material         %
%   of the paper and also available at:                                          %
%                                                                                   %
%           https://github.com/PrabhatIn/SoRoTop   %
%                                                                                   %
%   Please send your comment to: pkumar@mae.iith.ac.in                           %
%                                                                                   %
%   One may also refer to the following two papers for more detail:              %
%                                                                                   %
%   1. Kumar P, Frouws JS, Langelaar M (2020) Topology optimization of fluidic    %
%   pressure-loaded structures and compliant mechanisms using the Darcy method.  %
%   Structural and Multidisciplinary Optimization 61(4):1637-1655                %
%   2. Kumar P, Langelaar M (2021) On topology optimization of design-dependent   %
%   pressure-loaded three-dimensional structures and compliant mechanisms.       %
%   International Journal for Numerical Methods in Engineering 122(9):2205-2220  %
%   3. P. Kumar (2023) TOPress: a MATLAB implementation for topology optimization %
%   of structures subjected to desig-dependent pressure loads, Structural and    %
%   Multidisciplinary Optimization, 66(4), 2023                                %
%                                                                                   %
%                                                                                   %
%   Disclaimer:                                                                     %
%   The author does not guarantee that the code is free from erros but reserves %
%   all rights. Further, the author shall not be liable in any event caused by  %
%   use of the above code and its extensions                                     %
%                                                                                   %
%%%%%%%%%%%%%%%%%%%%%%%%%%%%%%%%%%%%%%%%%%%%%%%%%%%%%%%%%%%%%%%%%%%%%%%%%%

```

## References

- Alexandersen J (2023) A detailed introduction to density-based topology optimisation of fluid flow problems with implementation in MATLAB. *Structural and Multidisciplinary Optimization* 66(1):1–38
- Ali MA, Shimoda M (2022) Toward multiphysics multiscale concurrent topology optimization for lightweight structures with high heat conductivity and high stiffness using MATLAB. *Structural and Multidisciplinary Optimization* 65(7):1–26
- Andreassen E, Clausen A, Schevenels M, Lazarov BS, Sigmund O (2011) Efficient topology optimization in MATLAB using 88 lines of code. *Structural and Multidisciplinary Optimization* 43(1):1–16
- Bruns TE, Tortorelli DA (2001) Topology optimization of non-linear elastic structures and compliant mechanisms. *Comput Method Appl Mech Eng* 190(26-27):3443–3459
- Chen F, Xu W, Zhang H, Wang Y, Cao J, Wang MY, Ren H, Zhu J, Zhang Y (2018) Topology optimized design, fabrication, and characterization of a soft cable-driven gripper. *IEEE Robotics and Automation Letters* 3(3):2463–2470
- Deimel R, Brock O (2013) A compliant hand based on a novel pneumatic actuator. In: 2013 IEEE International Conference on Robotics and Automation, IEEE, pp 2047–2053
- Fernández E, Yang Kk, Koppen S, Alarcón P, Bauduin S, Duysinx P (2020) Imposing minimum and maximum member size, minimum cavity size, and minimum separation distance between solid members in topology optimization. *Computer Methods in Applied Mechanics and Engineering* 368:113157
- Ferrari F, Sigmund O, Guest JK (2021) Topology optimization with linearized buckling criteria in 250 lines of matlab. *Structural and Multidisciplinary Optimization* 63(6):3045–3066
- Gao J, Luo Z, Xia L, Gao L (2019) Concurrent topology optimization of multiscale composite structures in matlab. *Structural and Multidisciplinary Optimization* 60(6):2621–2651

- Gorissen B, Reynaerts D, Konishi S, Yoshida K, Kim JW, De Volder M (2017) Elastic inflatable actuators for soft robotic applications. *Advanced Materials* 29(43):1604977
- Hammer VB, Olhoff N (2000) Topology optimization of continuum structures subjected to pressure loading. *Structural and Multidisciplinary Optimization* 19(2):85–92
- Hiller J, Lipson H (2011) Automatic design and manufacture of soft robots. *IEEE Transactions on Robotics* 28(2):457–466
- Homayouni-Amlashi A, Schlienger T, Mohand-Ousaid A, Rakotondrabe M (2021) 2D topology optimization MATLAB codes for piezoelectric actuators and energy harvesters. *Structural and Multidisciplinary Optimization* 63(2):983–1014
- Hu X, Chen A, Luo Y, Zhang C, Zhang E (2018) Steerable catheters for minimally invasive surgery: a review and future directions. *Computer Assisted Surgery* 23(1):21–41
- Jin H, Dong E, Xu M, Liu C, Alici G, Jie Y (2016) Soft and smart modular structures actuated by shape memory alloy (sma) wires as tentacles of soft robots. *Smart Materials and Structures* 25(8):085026
- Kumar P (2022) Towards topology optimization of pressure-driven soft robots. In: *Microactuators, Microsensors and Micromechanisms: MAMM 2022*, Springer, pp 19–30
- Kumar P (2023) HoneyTop90: A 90-line MATLAB code for topology optimization using honeycomb tessellation. *Optimization and Engineering* 24(2):1433–1460
- Kumar P (2023) TOPress: a MATLAB implementation for topology optimization of structures subjected to design-dependent pressure loads. *Structural and Multidisciplinary Optimization* 66(4)
- Kumar P, Langelaar M (2021) On topology optimization of design-dependent pressure-loaded three-dimensional structures and compliant mechanisms. *International Journal for Numerical Methods in Engineering* 122(9):2205–2220
- Kumar P, Langelaar M (2022) Topological synthesis of fluidic pressure-actuated robust compliant mechanisms. *Mechanism and Machine Theory* 174:104871
- Kumar P, Saxena A (2022) An improved material mask overlay strategy for the desired discreteness of pressure-loaded optimized topologies. *Structural and Multidisciplinary Optimization* 65(10):304
- Kumar P, Saxena A, Sauer RA (2019) Computational synthesis of large deformation compliant mechanisms undergoing self and mutual contact. *Journal of Mechanical Design* 141(1)
- Kumar P, Frouws JS, Langelaar M (2020) Topology optimization of fluidic pressure-loaded structures and compliant mechanisms using the Darcy method. *Structural and Multidisciplinary Optimization* 61(4):1637–1655
- Kumar P, Schmidleithner C, Larsen N, Sigmund O (2021) Topology optimization and 3D printing of large deformation compliant mechanisms for straining biological tissues. *Structural and Multidisciplinary Optimization* 63:1351–1366
- Lu Y, Tong L (2021) Topology optimization of compliant mechanisms and structures subjected to design-dependent pressure loadings. *Structural and Multidisciplinary Optimization* 63(4):1889–1906
- Lu Y, Tong L (2022) Optimal design and experimental validation of 3D printed soft pneumatic actuators. *Smart Materials and Structures* 31(11):115010
- Moscatelli E, Sá LF, Emmendoerfer Jr H, Silva EC (2023) Pure-displacement formulation and bulk modulus propagation for topology optimization with pressure loads. *Computer Methods in Applied Mechanics and Engineering* 411:116058



- Panganiban H, Jang GW, Chung TJ (2010) Topology optimization of pressure-actuated compliant mechanisms. *Finite Elements in Analysis and Design* 46(3):238–246
- Picelli R, Neofytou A, Kim HA (2019) Topology optimization for design-dependent hydrostatic pressure loading via the level-set method. *Structural and Multidisciplinary Optimization* 60(4):1313–1326
- Picelli R, Sivapuram R, Xie YM (2021) A 101-line MATLAB code for topology optimization using binary variables and integer programming. *Structural and Multidisciplinary Optimization* 63(2):935–954
- Pinskier J, Kumar P, Langelaar M, Howard D (2023) Automated design of pneumatic soft grippers through design-dependent multi-material topology optimization. In: 6th IEEE-RAS International Conference on Soft Robotics (RoboSoft 2023), IEEE
- Polygerinos P, Lyne S, Wang Z, Nicolini LF, Mosadegh B, Whitesides GM, Walsh CJ (2013) Towards a soft pneumatic glove for hand rehabilitation. In: 2013 IEEE/RSJ International Conference on Intelligent Robots and Systems, IEEE, pp 1512–1517
- Poulsen TA (2003) A new scheme for imposing a minimum length scale in topology optimization. *International Journal for Numerical Methods in Engineering* 57(6):741–760
- Pourazadi S, Bui H, Menon C (2019) Investigation on a soft grasping gripper based on dielectric elastomer actuators. *Smart Materials and Structures* 28(3):035009
- Saxena A, Ananthasuresh GK (2000) On an optimal property of compliant topologies. *Structural and multidisciplinary optimization* 19(1):36–49
- Saxena R, Saxena A (2007) On honeycomb representation and sigmoid material assignment in optimal topology synthesis of compliant mechanisms. *Finite Elements in Analysis and Design* 43(14):1082–1098
- Shintake J, Cacucciolo V, Floreano D, Shea H (2018) Soft robotic grippers. *Advanced materials* 30(29):1707035
- Sigmund O (1997) On the design of compliant mechanisms using topology optimization. *Journal of Structural Mechanics* 25(4):493–524
- Sigmund O (2001) A 99 line topology optimization code written in matlab. *Structural and multidisciplinary optimization* 21(2):120–127
- Sigmund O, Maute K (2013) Topology optimization approaches. *Structural and Multidisciplinary Optimization* 48(6):1031–1055
- Singh N, Kumar P, Saxena A (2020) On topology optimization with elliptical masks and honeycomb tessellation with explicit length scale constraints. *Structural and Multidisciplinary Optimization* 62:1227–1251
- de Souza EM, Silva ECN (2020) Topology optimization applied to the design of actuators driven by pressure loads. *Structural and Multidisciplinary Optimization* 61(5):1763–1786
- Suresh K (2010) A 199-line matlab code for pareto-optimal tracing in topology optimization. *Structural and Multidisciplinary Optimization* 42:665–679
- Svanberg K (1987) The method of moving asymptotes—a new method for structural optimization. *Int J Numer Meth Eng* 24(2):359–373
- Svanberg K (2007) MMA and GCMMA—two methods for nonlinear optimization. vol 1:1–15
- Vasista S, Tong L (2012) Design and testing of pressurized cellular planar morphing structures. *AIAA journal* 50(6):1328–1338

- Wang C, Zhao Z, Zhou M, Sigmund O, Zhang XS (2021) A comprehensive review of educational articles on structural and multidisciplinary optimization. *Structural and Multidisciplinary Optimization* 64(5):2827–2880
- Wang F, Lazarov BS, Sigmund O (2011) On projection methods, convergence and robust formulations in topology optimization. *Structural and multidisciplinary optimization* 43:767–784
- Wang F, Lazarov BS, Sigmund O, Jensen JS (2014) Interpolation scheme for fictitious domain techniques and topology optimization of finite strain elastic problems. *Computer Methods in Applied Mechanics and Engineering* 276:453–472
- Xavier MS, Tawk CD, Zolfagharian A, Pinskiar J, Howard D, Young T, Lai J, Harrison SM, Yong YK, Bodaghi M (2022) Soft pneumatic actuators: A review of design, fabrication, modeling, sensing, control and applications. *IEEE Access*
- Xie Z, Domel AG, An N, Green C, Gong Z, Wang T, Knubben EM, Weaver JC, Bertoldi K, Wen L (2020) Octopus arm-inspired tapered soft actuators with suckers for improved grasping. *Soft robotics* 7(5):639–648
- Yin L, Ananthasuresh G (2003) Design of distributed compliant mechanisms. *Mechanics based design of structures and machines* 31(2):151–179
- Zhang H, Kumar AS, Fuh JYH, Wang MY (2018) Design and development of a topology-optimized three-dimensional printed soft gripper. *Soft robotics* 5(5):650–661
- Zhao H, O'Brien K, Li S, Shepherd RF (2016) Optoelectronically innervated soft prosthetic hand via stretchable optical waveguides. *Science robotics* 1(1):eaai7529